

AD\_\_\_\_\_

Award Number: DAMD17-03-1-0143

TITLE: Imaging Primary Prostate Cancer and Bone Metastasis

PRINCIPAL INVESTIGATOR: Xiaoyuan Chen, Ph.D.

CONTRACTING ORGANIZATION: Stanford University  
Stanford, California 94305-4125

REPORT DATE: April 2006

TYPE OF REPORT: Annual

PREPARED FOR: U.S. Army Medical Research and Materiel Command  
Fort Detrick, Maryland 21702-5012

DISTRIBUTION STATEMENT: Approved for Public Release;  
Distribution Unlimited

The views, opinions and/or findings contained in this report are those of the author(s) and should not be construed as an official Department of the Army position, policy or decision unless so designated by other documentation.

REPORT DOCUMENTATION PAGE				Form Approved OMB No. 0704-0188	
Public reporting burden for this collection of information is estimated to average 1 hour per response, including the time for reviewing instructions, searching existing data sources, gathering and maintaining the data needed, and completing and reviewing this collection of information. Send comments regarding this burden estimate or any other aspect of this collection of information, including suggestions for reducing this burden to Department of Defense, Washington Headquarters Services, Directorate for Information Operations and Reports (0704-0188), 1215 Jefferson Davis Highway, Suite 1204, Arlington, VA 22202-4302. Respondents should be aware that notwithstanding any other provision of law, no person shall be subject to any penalty for failing to comply with a collection of information if it does not display a currently valid OMB control number. <b>PLEASE DO NOT RETURN YOUR FORM TO THE ABOVE ADDRESS.</b>					
1. REPORT DATE (DD-MM-YYYY) 01-04-2006		2. REPORT TYPE Annual		3. DATES COVERED (From - To) 1 Apr 2004 – 31 Mar 2006	
4. TITLE AND SUBTITLE  Imaging Primary Prostate Cancer and Bone Metastasis				5a. CONTRACT NUMBER	
				5b. GRANT NUMBER DAMD17-03-1-0143	
				5c. PROGRAM ELEMENT NUMBER	
6. AUTHOR(S)  Xiaoyuan Chen, Ph.D.  E-Mail: <a href="mailto:shawchen@stanford.edu">shawchen@stanford.edu</a>				5d. PROJECT NUMBER	
				5e. TASK NUMBER	
				5f. WORK UNIT NUMBER	
7. PERFORMING ORGANIZATION NAME(S) AND ADDRESS(ES)  Stanford University Stanford, California 94305-4125				8. PERFORMING ORGANIZATION REPORT NUMBER	
9. SPONSORING / MONITORING AGENCY NAME(S) AND ADDRESS(ES) U.S. Army Medical Research and Materiel Command Fort Detrick, Maryland 21702-5012				10. SPONSOR/MONITOR'S ACRONYM(S)	
				11. SPONSOR/MONITOR'S REPORT NUMBER(S)	
12. DISTRIBUTION / AVAILABILITY STATEMENT Approved for Public Release; Distribution Unlimited					
13. SUPPLEMENTARY NOTES					
14. ABSTRACT The overall objective of the proposed research is to develop positron emitter labeled bombesin (BBN) analogs with high affinity for the GRP receptor GRPR for microPET imaging of both androgen dependent and androgen independent prostate cancer xenografted mice. Specific Aims: (1) Design, synthesize, and characterize positron emitting bombesin analogs, labeled with copper-64 or fluorine-18; (2) Conduct in vitro studies of copper-64 and fluorine-18 labeled bombesin analogs to evaluate the effect of modification and radiolabeling on the receptor binding affinity and specificity; (3) Evaluate in vivo efficacy of these novel radiopharmaceuticals in the murine PC-3 and CWR22 human prostate cancer xenograft models. Major Findings: In year 1, we coupled Lys3-BBN with DOTA and labeled the DOTA-Lys3-BBN conjugate with 64Cu for imaging both subcutaneous PC-3 (GRPR+) and CWR22 (GRPR-) tumors. In year 2, we further tested a series of BBN analogs and fully characterized 64Cu-DOTA-Aca-BBN(7-14). Studies on metabolic stability for both tracers on organ homogenates showed that 64Cu-DOTA-[Lys3]BBN is relatively stable. This study demonstrated that both tracers are suitable for targeted PET imaging to detect the expression of GRPR in prostate cancer, while 64Cu-DOTA-[Lys3]BBN may have a better potential for clinical translation.					
15. SUBJECT TERMS No subject terms provided.					
16. SECURITY CLASSIFICATION OF:			17. LIMITATION OF ABSTRACT	18. NUMBER OF PAGES	19a. NAME OF RESPONSIBLE PERSON
a. REPORT	b. ABSTRACT	c. THIS PAGE			USAMRMC
U	U	U	UU	34	19b. TELEPHONE NUMBER (include area code)

## Table of Contents

<b>Introduction.....</b>	<b>4</b>
<b>Body.....</b>	<b>5</b>
<b>Key Research Accomplishments.....</b>	<b>12</b>
<b>Reportable Outcomes.....</b>	<b>13</b>
<b>Conclusions.....</b>	<b>14</b>
<b>References.....</b>	<b>15</b>
<b>Appendices.....</b>	<b>16</b>

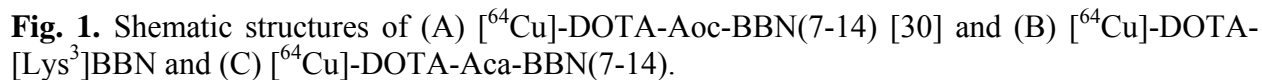
## INTRODUCTION

Although gastrin releasing peptide (GRP) receptors are known to be overexpressed in human neoplastic prostate tissues, little has been published on the development of radiopharmaceuticals for systemic evaluation of GRP receptor agonists and antagonists. The overall objective of the proposed research is to develop positron emitter labeled bombesin analogs with high affinity for the GRP receptor GRPR for microPET imaging of both androgen dependent and androgen independent prostate cancer xenografted mice. **Specific Aims:** (1) Design, synthesize, and characterize positron emitting bombesin analogs, labeled with copper-64 or fluorine-18; (2) Conduct *in vitro* studies of copper-64 and fluorine-18 labeled bombesin analogs to evaluate the effect of modification and radiolabeling on the receptor binding affinity and specificity; (3) Evaluate *in vivo* efficacy of these novel radiopharmaceuticals in the murine PC-3 and 22Rv1 human prostate cancer xenograft models.

We have previously demonstrated the feasibility of the PET imaging using  $^{64}\text{Cu}$ -DOTA-[Lys<sup>3</sup>]BBN to detect GRPR-positive prostate cancer (Annual report for Year 1) (1). Rogers et. al. (2) developed a truncated form of a  $^{64}\text{Cu}$ -labeled BBN analogue,  $^{64}\text{Cu}$ -DOTA-Aoc-BBN(7-14). The study showed that this truncated BBN peptide with an alkyl linker has high affinity and internalization on GRP-positive cells (Fig. 1A). It also showed successful targeting and accumulation in PC-3 tumor. Alternatively, a poly(ethylene glycol) (PEG) linker (M.W. = 3,400) resulted in significantly reduced receptor affinity and lower receptor specific activity accumulation *in vivo* (3). However, it is unclear whether the C-terminal fragment or the full length of the amphibian tetradecapeptide bombesin is more suitable for GRPR targeting *in vivo*. In order to investigate the nature of these two types of BBN analogues, in this study we continued to characterize  $^{64}\text{Cu}$ -DOTA-[Lys<sup>3</sup>]BBN, and extended the methodology to  $^{64}\text{Cu}$ -DOTA-Aca-BBN(7-14), where Aca refers to  $\epsilon$ -aminocaproic acid. For both compounds, *in vitro* assays, metabolic stability, and microPET studies were performed to investigate tumor targeting and *in vivo* kinetics (4).

## Chemistry and Radiochemistry

**A**



### *In vitro receptor binding assay*

The binding affinity of [Lys<sup>3</sup>]BBN, Aca-BBN(7-14) and DOTA-Aca-BBN(7-14) for GRPR was evaluated for PC-3 and 22Rv1 human prostate adenocarcinoma cell lines. A typical sigmoid curve for the displacement of <sup>125</sup>I-[Tyr<sup>4</sup>]BBN from PC-3 cells as a function of increasing concentration of DOTA-Aca-BBN(7-14) was obtained. The IC<sub>50</sub> values (concentration required to have 50% inhibitory effect) were determined for all three different ligands on both PC-3 and 22Rv1 cells, and were summarized in Table 1. The IC<sub>50</sub> value was determined to be  $3.3 \pm 0.4$  nM for [Lys<sup>3</sup>]BBN and  $20.8 \pm 0.3$  nM for Aca-BBN(7-14) on  $10^5$  PC-3 cells. Conjugation with DOTA did not significantly alter the binding affinity for both compounds. The results showed the IC<sub>50</sub> values to be  $2.2 \pm 0.5$  and  $18.4 \pm 0.2$  nM for DOTA-[Lys<sup>3</sup>]BBN and DOTA-Aca-BBN(7-14), respectively. For 22Rv1, no significant binding characteristics could be obtained for any of the four compounds with the use of up to  $2.5 \times 10^5$  cells. The binding affinity of [Tyr<sup>4</sup>]BBN for GRPR was also evaluated for PC-3 and 22Rv1 cell lines against <sup>125</sup>I-[Tyr<sup>4</sup>]BBN to estimate the receptor density on the cells. A sigmoid curve from PC-3 cells as a function of increasing concentration of [Tyr<sup>4</sup>]BBN was obtained. The linear portion of the data was used to generate the Scatchard transformation.  $K_d$  (the mean dissociation constant between the radioligand and the GRPR on the cell surface) of <sup>125</sup>I-[Tyr<sup>4</sup>]BBN against PC-3 cells was calculated to be  $14.8 \pm 0.4$  nM and  $B_{max}$ , the density of GRPR on cell surface to be  $2.7 \pm 0.1 \times 10^6$  receptors/cell. For 22Rv1, no significant binding affinity could be obtained.

**Table 1.** Summary of (A) the IC<sub>50</sub> values for different ligands against PC-3 and 22Rv1 cell lines obtained from competitive binding assay using <sup>125</sup>I-[Tyr<sup>4</sup>]BBN; (B)  $K_d$  and  $B_{Max}$  for PC-3 and 22Rv1 cell lines measured using [Tyr<sup>4</sup>]-BBN obtained from the saturation binding curve using Scatchard transformation of the competitive binding curve.

(A) IC <sub>50</sub> (nmol/L)	PC-3	22Rv1
[Lys <sup>3</sup> ]-BBN	$3.3 \pm 0.4$	NS <sup>1</sup>
DOTA-[Lys <sup>3</sup> ]-BBN	$2.2 \pm 0.5$	NS <sup>1</sup>
Aca-BBN(7-14)	$20.8 \pm 0.3$	NS <sup>1</sup>
DOTA-Aca-BBN(7-14)	$18.4 \pm 0.2$	NS <sup>1</sup>
(B)	PC-3	22Rv1
$K_d$ (nM)	$14.8 \pm 0.4$	NS <sup>1</sup>
$B_{Max}$ (receptors/cell)	$2.70 \pm 0.1 \times 10^6$	NS <sup>1</sup>

<sup>1</sup> NS: readings from gamma-counter are not significant enough to extract a binding curve and associated parameters.

## Internalization and efflux studies

Results for the internalization of both tracers, [ $^{64}\text{Cu}$ ]-DOTA-[Lys<sup>3</sup>]BBN and [ $^{64}\text{Cu}$ ]-DOTA-Aca-BBN(7-14), were shown in Fig. 2A. For both tracers, internalization occurred immediately after the pre-incubation step (at 0 min of incubation): 55% for [ $^{64}\text{Cu}$ ]-DOTA-[Lys<sup>3</sup>]BBN and 60% for [ $^{64}\text{Cu}$ ]-DOTA-Aca-BBN(7-14). At approximately 20 minutes of incubation, internalization for both tracers reached a maximum (~84% for [ $^{64}\text{Cu}$ ]-DOTA-[Lys<sup>3</sup>]BBN and >75% for [ $^{64}\text{Cu}$ ]-DOTA-Aca-BBN(7-14)) and stayed saturated up till 120 minutes of incubation.

Efflux studies were also carried out up to 24 hours of incubation to further characterize both tracers (Fig. 2B). Both [ $^{64}\text{Cu}$ ]-DOTA-[Lys<sup>3</sup>]BBN and [ $^{64}\text{Cu}$ ]-DOTA-Aca-BBN(7-14) tracers showed a similar efflux curve: with 30 minutes of incubation, both tracers had approximately 20-25% efflux out of the PC-3 cells, followed by a ~15% increase up till 4 hours of incubation. The efflux rate was decreased afterwards. Till the end of experiments with a 24 hour incubation time, approximately 40% of the radiotracers remained in the cells.

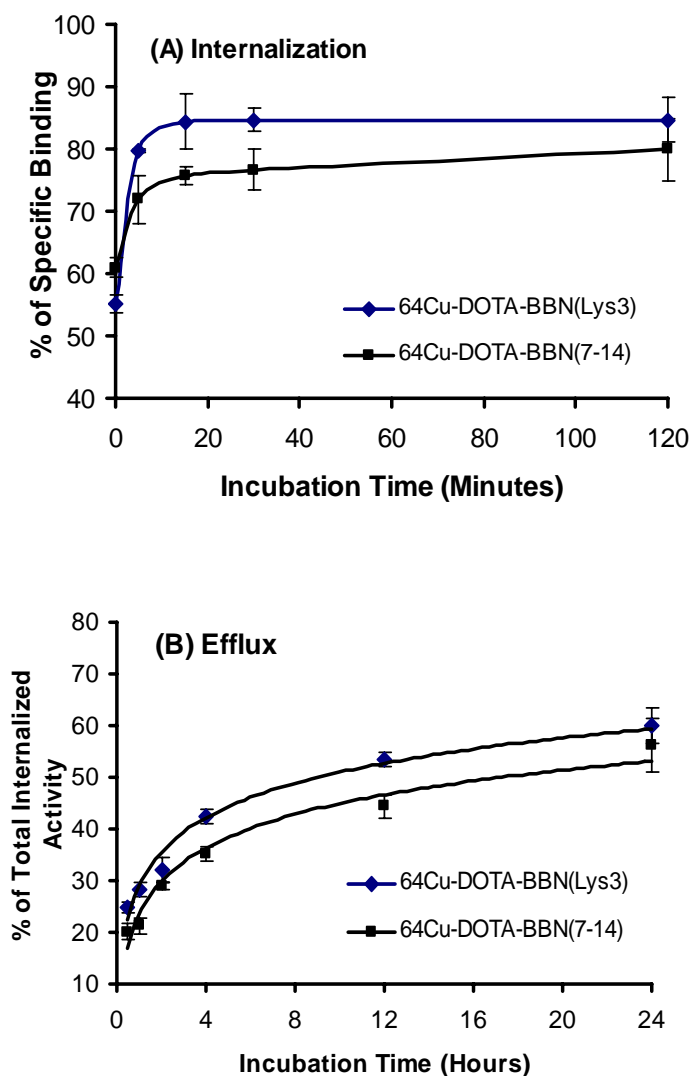


**Fig. 2.** (A) Time-dependent internalization and (B) time-dependent efflux of [ $^{64}\text{Cu}$ ]-DOTA-[Lys<sup>3</sup>]BBN (♦) and [ $^{64}\text{Cu}$ ]-DOTA-Aca-BBN(7-14) (■) by PC-3 cells. Data are percentage of acid-resistant (internalized) radio-activity in cells for internalization, and percentage of radio-activity remained in the culture media for efflux.

### *Metabolism stability*

The metabolic stability of [ $^{64}\text{Cu}$ ]-DOTA-[Lys<sup>3</sup>]BBN was determined in mouse blood, urine, tumor, liver and kidney samples 30, 60 min and 120 min (data not shown) p.i. Efficiency of extraction by homogenizing the organs and efficiency of elution was summarized in Table 2A; and Table 3A summarizes the relative integrated area of each individual peaks in percentage for [ $^{64}\text{Cu}$ ]-DOTA-[Lys<sup>3</sup>]BBN. HPLC of the radio-labeled tracer performed immediately prior to the injection showed a single peak (100% area) with a retention time of 18.5 min. This spectrum was used as the 0 min time point for blood, urine and all the organ samples. At 30 min p.i., approximately 78% of the intact tracer was retained in the blood and a new peak at about 5 minutes showed up with 22% area. Approximately 65% of the intact tracer was detected in tumor along with the second metabolite at 6 min. Liver had about 65% of the intact tracer; and in addition to the metabolite eluted at early time (4.0 min, 12%), a third peak was observable at 14 min with an area of about 23%. For kidneys, there was less than 30% of the intact tracer found. The major peak (72%) was observed at 4 minutes. A complete metabolism was observed in urine (100% area at 5.0 min).

HPLC at 60 min p.i. showed an increasing area for the early time eluent(s), indicating that the tracer had been further metabolized. For blood, the intact tracer decreased to < 60% and it further dropped to 23%, 40% and 17% in tumor, liver and kidneys, respectively. The second metabolite eluted at about 14 minutes for liver remained observable with an increasing area (from 23% to 43%). In urine, two peaks were observed at 3 and 4 min, likely to be new metabolites derived from the one eluted at 5 min at 30 min p.i. HPLC for samples collected at 120 min p.i. showed further decomposition of the radio-labeled tracer (data not shown).

The metabolic stability of [ $^{64}\text{Cu}$ ]-DOTA-Aca-BBN(7-14) was also determined in mouse blood, urine, tumor, liver and kidney samples 30 and 60 min p.i. using the same protocol. Efficiency of extraction by homogenizing the organs was 97.8% to 81.6%, and efficiency of elution was between 96.1% and 75.0%, as shown in Table 2B. Table 3B summarizes the relative integrated area for each individual peaks in percentage for [ $^{64}\text{Cu}$ ]-DOTA-Aca-BBN(7-14). HPLC of the radio-labeled tracer was performed immediately before the tracer injection as the 0 min data point for all 5 extractants. It showed that the intact tracer had an elution time of approximately 18 min. HPLC of those samples were performed, eluents were collected every 30 seconds for gamma counting and the HPLC spectra were reconstructed using the counting results for 30 and 60 min.

At 30 min p.i., the peak for intact tracer was not observable in any of the 5 samples. Blood sample showed two broad bands at 19.5 (68%) and at 4-5 minutes (total 32%). Urine and PC-3 tumor samples showed one peak at 14.5 min and another weak peak at 4-5 min with higher intensity. Liver and kidney samples showed a group of broad bands with identifiable peaks at about 19, 15 (major peak for liver, 45% area) and 4 min (major peak for kidney, 52% area). At 60 min and 120 min (data not shown) p.i., HPLC spectra showed a further metabolism for the injected radio-tracer with no sign of the intact tracer at 18.0 min retention time. Peaks at areas of low retention time showed increased % area. For blood and liver, broader band consisted of multiple peaks was also observed.



Together these results for both [ $^{64}\text{Cu}$ ]-DOTA-[Lys<sup>3</sup>]BBN and [ $^{64}\text{Cu}$ ]-DOTA-Aca-BBN(7-14) showed that [ $^{64}\text{Cu}$ ]-DOTA-Aca-BBN(7-14) has extremely low metabolic stability as the tracer decomposed sooner than 30 min after being injected. Alternatively, [ $^{64}\text{Cu}$ ]-DOTA-[Lys<sup>3</sup>]BBN showed a moderate metabolic stability. At 60 min p.i., approximately 23% of the tracer remained in the tumor. Further work has yet to be accomplished to identify the metabolites observed in these experiments.

**Table 2.** Summary of the extraction and elution efficiency from blood, urine, liver, kidney and PC-3 tumor collected at 30 and 60 minutes post intravenous injection of (A) [ $^{64}\text{Cu}$ ]-DOTA-[Lys<sup>3</sup>]-BBN and (B) [ $^{64}\text{Cu}$ ]-DOTA-Aca-BBN(7-14).

(A) [ $^{64}\text{Cu}$ ]-DOTA-[Lys <sup>3</sup> ]-BBN										
	Extraction Efficiency (%)					Elution Efficiency (%)				
	Blood	Urine	Liver	Kidney	Tumor	Blood	Urine	Liver	Kidney	Tumor
30 mins p.i.	92.7	N/A	78.3	70.7	76.9	94.4	96.0	84.6	88.6	88.0
60 mins p.i.	87.6	N/A	71.5	60.8	85.3	95.9	97.0	90.3	88.9	95.9

(B) [ $^{64}\text{Cu}$ ]-DOTA-Aca-BBN(7-14)										
	Extraction Efficiency (%)					Elution Efficiency (%)				
	Blood	Urine	Liver	Kidney	Tumor	Blood	Urine	Liver	Kidney	Tumor
30 mins p.i.	97.8	N/A	93.9	89.6	81.6	93.6	90.7	88.7	84.5	75.0
60 mins p.i.	96.1	N/A	90.5	89.6	85.8	96.1	92.8	84.6	83.8	80.3

**Table 3.** Summary of data from the HPLC profiles shown in Figure 4 from the soluble fraction of blood and urine samples and organ homogenates 0 (immediately prior to injection), 30 and 60 minutes post intravenous injection of (A) [ $^{64}\text{Cu}$ ]-DOTA-[Lys<sup>3</sup>]-BBN and (B) [ $^{64}\text{Cu}$ ]-DOTA-Aca-BBN(7-14).

A	Blood		Urine		Tumor		Liver		Kidney	
	Elution time (mins)	Area (%)	Elution time (mins)	Area (%)	Elution time (mins)	Area (%)	Elution time (mins)	Area (%)	Elution time (mins)	Area (%)
	18.5	100	18.5	100	18.5	100	18.5	100	18.5	100
	18.5	78.0			18.5	64.6	18.5	65.4	18.5	25.9
							14.0	23.4		
	5.0	22.0	5.0	100	6.0	35.4	4.0	11.2	4.0	72.1
	18.5	58.4			18.5	23.1	18.5	39.9	18.5	17.4
							14.0	43.4		
	3.0	42.6	3.0	65.2	6.0	76.9	4.0	16.7	4.0	82.6
			4.0	34.8						

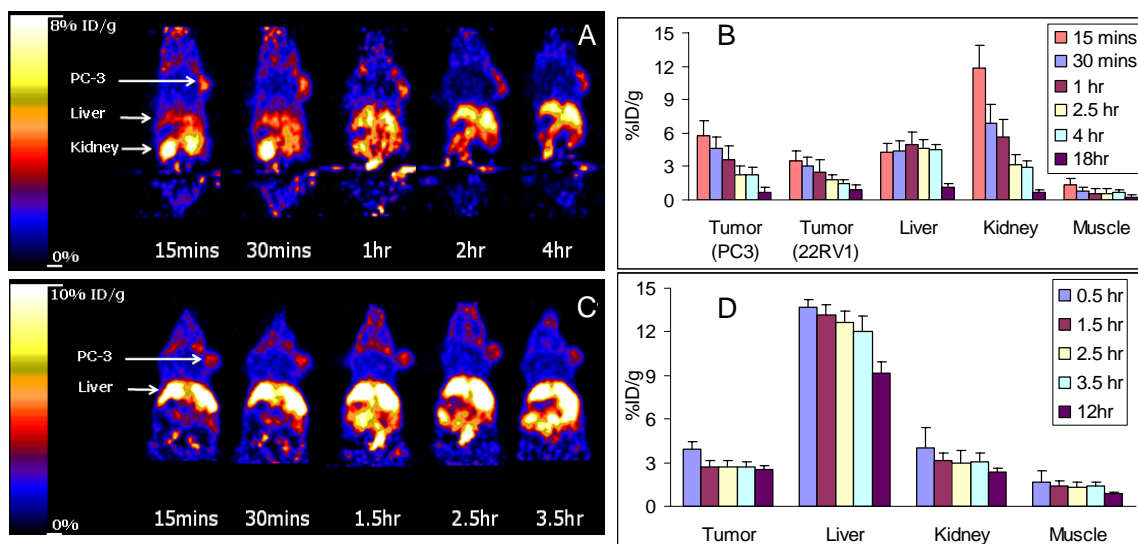
  

B	Blood		Urine		Tumor		Liver		Kidney	
	Elution time (mins)	Area (%)	Elution time (mins)	Area (%)	Elution time (mins)	Area (%)	Elution time (mins)	Area (%)	Elution time (mins)	Area (%)
	18.0	100	18.0	100	18.0	100	18.0	100	18.0	100
	19.0	68.1					19.0	20.1	19.5	45.2
			14.5	39.4	14.5	65.3	15.0	45.3		
	5.5	21.4	5.0	60.6	4.0	34.7	4.0	33.5	4.0	51.9
	4.0	10.5								
	18.5	14.2								
					14.5	56.9	13.5	45.1		
	6.0	41.4	4.0	100	4.0	43.1	5.0	52.9	4.0	100
	3.5	44.8								

## MicroPET imaging

Fig. 3A showed a series of microPET images of a nude mouse bearing PC-3 tumor on the right shoulder and 22Rv1 tumor on the left shoulder (not seen from the coronal images shown) after injecting approximately 300  $\mu$ Ci (11.1 MBq) of [ $^{64}$ Cu]-DOTA-[Lys<sup>3</sup>]BBN. The data were collected using a dynamic sequence from 0 to 60 min, and a static sequence at 2, 4, 12 and 18 hours p.i (data acquisition protocol was described in the Material and Methods section). Quantification of tracer uptake in %ID/g was calculated and shown in Fig. 3B. It has been shown that tracer uptake calculated from non-invasive microPET imaging is comparable to that obtained from direct tissue sampling [29]. Uptake of [ $^{64}$ Cu]-DOTA-[Lys<sup>3</sup>]BBN occurred immediately after injection for both tumors and all the organs. Maximum uptake was observed at 15 min for both tumors, kidneys and muscle. Uptake in the liver reached its maximum level at about 1 h p.i. Uptake in PC-3 tumor is higher than that in 22Rv1 tumor (%ID/g = 5.8 for PC-3 and 3.49,  $p < 0.01$ ), demonstrating that this tracer was able to target the GRPR whose expression level is high in PC-3 but low in 22Rv1 tumor. It also should be noted that kidney uptake was the highest among all the ROIs studied here, suggesting that excretion through the kidney/urine is likely to be the pathway for this tracer to be metabolized.

Significant difference in uptake behavior was observed for [ $^{64}$ Cu]-DOTA-Aca-BBN(7-14) compared to that for [ $^{64}$ Cu]-DOTA-[Lys<sup>3</sup>]BBN (Fig. 3C and D). Uptake on PC-3 tumor reached maximum (4.63%) at around 5 min post injection and remained to be below 3% after 30 minutes post injection. Liver uptake was significantly higher than that for other organs and remained as high as 9%ID/g at 12 h p.i. Renal uptake was significantly lower than that for the previous tracer [ $^{64}$ Cu]-DOTA-[Lys<sup>3</sup>]BBN. When [ $^{64}$ Cu]-DOTA-Aca-BBN(7-14) was co-injected with blocking dose of [Tyr<sup>4</sup>]BBN (10 mg/kg), the activity accumulations in the PC-3 tumor and pancreas were partially inhibited, reflecting the low receptor affinity of the truncated peptide tracer (data not shown).



**Fig. 3.** MicroPET images of athymic nude mice with PC-3 tumor on the right shoulder. Coronal images (decayed corrected to time of injection) were collected at multiple time

points post radiotracer [ $^{64}\text{Cu}$ ]-DOTA-[Lys<sup>3</sup>]BBN (300  $\mu\text{Ci}$ , 11.1 MBq) (A) or [ $^{64}\text{Cu}$ ]-DOTA-Aca-BBN(7-14) (C) injection. Major organ and tumor distribution data derived from quantitative microPET imaging studies for [ $^{64}\text{Cu}$ ]-DOTA-[Lys<sup>3</sup>]BBN (B) and [ $^{64}\text{Cu}$ ]-DOTA-Aca-BBN(7-14) (D) were also shown ( $n = 3$ ). Time indicated in all panels refers to the time point of scan initiation.

## KEY ACCOMPLISHMENTS

- Several bombesin analogs have been labeled with positron emitter copper-64 ( $t_{1/2}$  = 12.8 h) with high receptor binding affinity and specificity;
- As compared to  $^{64}\text{Cu}$ -DOTA-Aca-BBN(7-14),  $^{64}\text{Cu}$ -DOTA-[Lys<sup>3</sup>]BBN has higher affinity for GRPR in vitro and metabolic stability in vivo, resulting in better imaging characteristics with higher tumor-to-background ratios;

## REPORTABLE OUTCOMES

### **Publications:**

Chen X, Park R, Hou Y, Tohme M, Shahinian AH, Bading JR, Conti PS  
MicroPET and Autoradiographic Imaging of GRP Receptor Expression with  $^{64}\text{Cu}$ -DOTA-[Lys<sup>3</sup>]bombesin in Human Prostate Adenocarcinoma Xenografts.  
*J Nucl Med* 2004;45:1390-1397 (Cover feature)

Yang Y-S, Zhang X, Xiong Z, Chen X.  
MicroPET imaging of gastrin-releasing peptide receptor expression with  $^{64}\text{Cu}$ -labeled bombesin analogs in a mouse model of human prostate adenocarcinoma.  
*Nucl Med Biol.* 2006;33:371-380.

### **Conference Abstracts:**

Chen X, Hou Y, Park R, Tohme M, Shahinian AH, Bading JR, Conti PS  
Evaluation of  $^{64}\text{Cu}$ -Labeled [Lys<sup>3</sup>]Bombesin as PET Tracer for Prostate Cancer GRP Receptor Imaging.  
AMI International Conference 2004, Orlando, FL, March, 2004.

Yang Y, Zhang X, Cheng Z, Chen X  
MicroPET Imaging of Gastrin-Releasing Peptide Receptor Expression with  $^{64}\text{Cu}$ -Labeled Bombesin Analogs in a Mouse Model of Human Prostate Adenocarcinoma.  
AMI International Conference 2005, Orlando, FL, March, 2005. (Abstract #: 320, poster)

Yang Y, Wu Y, Zhang X, Chen X  
NIR Fluorescence Imaging of Gastrin-Releasing Peptide Receptor Expression in Androgen-Independent Prostate Cancer Tumor Model.  
AMI International Conference 2005, Orlando, FL, March, 2005. (Abstract #: 321, poster)

### **Provisional Patent Application:**

PET imaging of gastrin releasing peptide receptors (GRPR) expression, compositions for GRPR cancer imaging, methods of GRPR cancer imaging.

## CONCLUSIONS

In conclusion, the data presented suggests that  $^{64}\text{Cu}$ -DOTA-[Lys<sup>3</sup>]BBN has high affinity for GRPR and moderate metabolic stability, results in specific tumor localization and exhibits good imaging characteristics with good tumor-to-background ratios.  $^{64}\text{Cu}$ -DOTA-[Lys<sup>3</sup>]BBN is also superior to  $^{64}\text{Cu}$ -DOTA-Aca-BBN[7-14] for GRPR positive tumor targeting.  $^{64}\text{Cu}$ -DOTA-[Lys<sup>3</sup>]BBN has the potential to be translated into clinical settings in healthy volunteers for defining tracer biodistribution, stability, pharmacokinetics and radiation dosimetry and in cancer patients for lesion detection and quantification of GRPR level.

## REFERENCES

1. Chen X, Park R, Hou Y, et al. microPET and autoradiographic imaging of GRP receptor expression with  $^{64}\text{Cu}$ -DOTA-[Lys3]bombesin in human prostate adenocarcinoma xenografts. *J Nucl Med.* Aug 2004;45(8):1390-1397.
2. Rogers BE, Bigott HM, McCarthy DW, et al. MicroPET imaging of a gastrin-releasing peptide receptor-positive tumor in a mouse model of human prostate cancer using a  $^{64}\text{Cu}$ -labeled bombesin analogue. *Bioconjug Chem.* Jul-Aug 2003;14(4):756-763.
3. Rogers BE, Manna DD, Safavy A. In vitro and in vivo evaluation of a  $^{64}\text{Cu}$ -labeled polyethylene glycol-bombesin conjugate. *Cancer Biother Radiopharm.* Feb 2004;19(1):25-34.
4. Yang YS, Zhang X, Xiong Z, Chen X. Comparative in vitro and in vivo evaluation of two  $^{64}\text{Cu}$ -labeled bombesin analogs in a mouse model of human prostate adenocarcinoma. *Nucl Med Biol.* Apr 2006;33(3):371-380.

## APPENDICES

Chen X, Park R, Hou Y, Tohme M, Shahinian AH, Bading JR, Conti PS  
MicroPET and Autoradiographic Imaging of GRP Receptor Expression with  $^{64}\text{Cu}$ -  
DOTA-[Lys<sup>3</sup>]bombesin in Human Prostate Adenocarcinoma Xenografts.  
*J Nucl Med* 2004;45:1390-1397 (Cover feature)

Yang Y-S, Zhang X, Xiong Z, Chen X.  
Comparative in vitro and in vivo evaluation of two  $^{64}\text{Cu}$ -labeled  
bombesin analogs in a mouse model of human prostate adenocarcinoma.  
*Nucl Med Biol.* 2006;33:371-380.



# microPET and Autoradiographic Imaging of GRP Receptor Expression with $^{64}\text{Cu}$ -DOTA-[Lys<sup>3</sup>]Bombesin in Human Prostate Adenocarcinoma Xenografts

Xiaoyuan Chen, PhD; Ryan Park, BS; Yingping Hou, MD; Michel Tohme, MS; Antranik H. Shahinian, BS; James R. Bading, PhD; and Peter S. Conti, MD, PhD

PET Imaging Science Center, University of Southern California Keck School of Medicine, Los Angeles, California

Overexpression of gastrin-releasing peptide (GRP) receptor (GRPR) in both androgen-dependent (AD) and androgen-independent (AI) human neoplastic prostate tissues provides an attractive target for prostate cancer imaging and therapy. The goal of this study was to develop  $^{64}\text{Cu}$ -radiolabeled GRP analogs for PET imaging of GRPR expression in prostate cancer xenografted mice. **Methods:** [Lys<sup>3</sup>]bombesin ([Lys<sup>3</sup>]BBN) was conjugated with 1,4,7,10-tetraazadodecane-*N,N',N'',N'''*-tetraacetic acid (DOTA) and labeled with the positron-emitting isotope  $^{64}\text{Cu}$  (half-life = 12.8 h, 19%  $\beta^+$ ). Receptor binding of DOTA-[Lys<sup>3</sup>]BBN and internalization of  $^{64}\text{Cu}$ -DOTA-[Lys<sup>3</sup>]BBN by PC-3 prostate cancer cells were measured. Tissue biodistribution, microPET, and whole-body autoradiographic imaging of the radiotracer were also investigated in PC-3 (AI)/CRW22 (AD) prostate cancer tumor models. **Results:** A competitive receptor-binding assay using [<sup>125</sup>I]-[Tyr<sup>4</sup>]BBN against PC-3 cells yielded a 50% inhibitory concentration value of  $2.2 \pm 0.5$  nmol/L for DOTA-[Lys<sup>3</sup>]BBN. Incubation of cells with the  $^{64}\text{Cu}$ -labeled radiotracer showed temperature- and time-dependent internalization. At 37°C, >60% of the tracer was internalized within the first 15 min and uptake remained constant for 2 h. Radiotracer uptake was higher in AI PC-3 tumor ( $5.62 \pm 0.08$  %ID/g at 30 min after injection, where %ID/g is the percentage of injected dose per gram) than in AD CWR22 tumor ( $1.75 \pm 0.05$  %ID/g at 30 min after injection). Significant accumulation of the activity in GRPR-positive pancreas was also observed ( $10.4 \pm 0.15$  %ID/g at 30 min after injection). Coinjection of a blocking dose of [Lys<sup>3</sup>]BBN inhibited the activity accumulation in PC-3 tumor and pancreas but not in CWR22 tumor. microPET and autoradiographic imaging of  $^{64}\text{Cu}$ -DOTA-[Lys<sup>3</sup>]BBN in athymic nude mice bearing subcutaneous PC-3 and CWR22 tumors showed strong tumor-to-background contrast. **Conclusion:** This study demonstrates that PET imaging of  $^{64}\text{Cu}$ -DOTA-[Lys<sup>3</sup>]BBN is able to detect GRPR-positive prostate cancer.

**Key Words:** prostate cancer; microPET; gastrin-releasing peptide receptor; bombesin;  $^{64}\text{Cu}$

**J Nucl Med 2004; 45:1390–1397**

A high-resolution and high-sensitivity nuclear medicine technique using radiopharmaceuticals that depict physiologic, metabolic, and molecular processes in vivo is PET. The most widely used agent is  $^{18}\text{F}$ -FDG, which accumulates in cells that have an increased metabolism due to increased need for or an inefficient glucose metabolism, such as cancer. Although  $^{18}\text{F}$ -FDG PET has been shown to effectively detect many types of primary tumors and metastases, it is not able to reliably differentiate benign hyperplasia and prostate cancer (1) or even to detect organ-confined carcinoma (2). Uptake of  $^{18}\text{F}$ -FDG in prostate carcinoma is generally low, apparently because the glucose utilization of prostate carcinoma cells is not enhanced significantly, compared with that of normal cells, to allow delineation of the tumor on the PET scan. Recent investigations of  $^{11}\text{C}$ -labeled (3,4) and  $^{18}\text{F}$ -labeled (5–8) choline and  $^{11}\text{C}$ -acetate (9–12) indicate that these agents hold promise in this disease. High expression of receptors on prostate cancer cells, as compared with normal prostate tissue and peripheral blood cells, provides the molecular basis for using radiolabeled receptor agonists or antagonists to visualize prostate tumors in nuclear medicine.  $^{18}\text{F}$ -Labeled androgens have been used to identify androgen-positive tissue in primates (13). Although this method is useful in determining if prostate cancer is hormone dependent, it does not provide a means for detecting tumors that are hormone independent. Thus, new markers that are able to identify the molecular determinants of prostate cancer development and progression regardless of androgen dependence need to be investigated.

The G protein-coupled gastrin-releasing peptide (GRP) receptor (GRPR) mediates the diverse actions of mammalian bombesin (BBN)-related peptide, GRP. In addition to

Received Dec. 1, 2003; revision accepted Feb. 5, 2004.  
For correspondence or reprints contact: Peter S. Conti, MD, PhD, Department of Radiology, University of Southern California, 1510 San Pablo St., Suite 350, Los Angeles, CA 90033.  
E-mail: pconti@usc.edu

its natural presence in the central nervous system and peripheral tissues, GRPR is overexpressed in several neuroendocrine tumors, including prostate cancer (14,15). In vitro receptor autoradiography of human nonneoplastic and neoplastic prostate tissue sections with  $^{125}\text{I}$ -[Tyr<sup>4</sup>]BBN as radioligand indicated high density of GRPR in well-differentiated carcinomas as well as bone metastases, but little or no GRPR was found in hyperplastic prostate and glandular tissue. This suggests that GRPR may be an indicator of early molecular events in prostate carcinogenesis and may be useful in differentiating prostate hyperplasia from neoplasia (14,15). GRPR-specific binding of  $^{125}\text{I}$ -[Tyr<sup>4</sup>]BBN was observed in human prostate cancer cell lines that are androgen independent (AI) but not in those that are androgen dependent (AD) (16). GRP promotes the growth and invasiveness of prostate cancer in vitro, and its secretion in vivo by endocrine cells is thought to be partially responsible for AI progression of the disease (17) by transactivation and up-regulation of epidermal growth factor receptors (18). Therefore, the use of GRPR antagonists or GRPR-targeting cytotoxic peptide conjugates could be an effective chemotherapeutic approach (19). In nuclear medicine, suitably radiolabeled BBN analogs have great potential for early noninvasive diagnosis as well as radiotherapy of prostate cancer (20,21).

$\gamma$ -Emitting  $^{99\text{m}}\text{Tc}$ -labeled BBN analogs have been synthesized and evaluated in vivo in normal mice (22,23) and PC-3 tumor-bearing mice (24,25) and have undergone feasibility testing in human patients (21). Although  $\gamma$ -emitters currently are more readily available relative to positron-emitting radionuclides ( $\beta^+$ ), the sensitivity of PET is at least 1–2 orders of magnitude better than that of single photon imaging systems (26). The acquisition of higher count statistics permits detection of smaller tumors for a given amount of radioactivity.

Recently, Rogers et al. (27) labeled DOTA-Aoc-BBN(7–14) (Aoc is 8-aminooctanoic acid) with  $^{64}\text{Cu}$  and applied this radiotracer to subcutaneous PC-3 xenografts. Although the tumor was well visualized, the sustained blood concentration and persistent liver and kidney retention limited potential clinical application of this tracer. In the present work, we evaluated the DOTA-[Lys<sup>3</sup>]BBN conjugate (DOTA is 1,4,7,10-tetraazadodecane-*N,N',N'',N'''*-tetraacetic acid) complexed with  $^{64}\text{Cu}$  for in vitro receptor-binding assay in PC-3 cells, for tumor targeting and in vivo kinetics by direct tissue sampling, and for visualization of prostate cancer tumors by microPET and whole-body autoradiography.

## MATERIALS AND METHODS

### Chemistry and Radiochemistry

[Lys<sup>3</sup>]BBN (American Peptide, Inc.) was conjugated with DOTA via in situ activation and coupling. Typically, DOTA, 1-ethyl-3-[3-(dimethylamino)propyl]carbodiimide (EDC), and *N*-hydroxysulfonosuccinimide (SNHS) at a molar ratio of DOTA:EDC:SNHS = 10:5:4 were mixed and reacted at 4°C for 30 min

(pH = 5.5). The sulfosuccinimidyl ester of DOTA (DOTA-OSSu) prepared without purification was then reacted with [Lys<sup>3</sup>]BBN in a theoretic stoichiometry of 5:1 and allowed to stand at 4°C overnight (pH 8.5–9.0). The DOTA-[Lys<sup>3</sup>]BBN conjugate was then purified by semipreparative high-performance liquid chromatography (HPLC) using a Waters 515 chromatography system with a Vydac protein and peptide column (218TP510; 5  $\mu\text{m}$ , 250  $\times$  10 mm). The flow was 3 mL/min, with the mobile phase starting from 95% solvent A (0.1% trifluoroacetic acid [TFA] in water) and 5% solvent B (0.1% TFA in acetonitrile) (0–2 min) to 35% solvent A and 65% solvent B at 32 min. The peak containing the DOTA conjugate was collected, lyophilized, and dissolved in H<sub>2</sub>O at a concentration of 1 mg/mL for use in radiolabeling reactions. Analytic HPLC was performed on the same pump system using a Vydac 218TP54 column (5  $\mu\text{m}$ , 250  $\times$  4.6 mm) and flow rate of 1 mL/min.

$^{64}\text{Cu}$  was produced on a CS-15 biomedical cyclotron at Washington University School of Medicine. The DOTA-[Lys<sup>3</sup>]BBN conjugate was labeled with  $^{64}\text{Cu}$  by addition of 37–185 MBq (1–5 mCi)  $^{64}\text{Cu}$  (2–5  $\mu\text{g}$  DOTA-[Lys<sup>3</sup>]BBN conjugate per MBq  $^{64}\text{Cu}$ ) in 0.1N NaOAc (pH 5.5) buffer followed by a 45-min incubation at 50°C. The reaction was terminated by adding 5  $\mu\text{L}$  of 10 mmol/L ethylenediaminetetraacetic acid solution, and radiochemical yield was determined by radio-TLC (TLC = thin-layer chromatography) using Whatman MKC18F TLC plates as the stationary phase and 70:30 MeOH:10% NaOAc as the eluent.  $^{64}\text{Cu}$ -DOTA-RGD was purified on a C<sub>18</sub> SepPak cartridge, using 85% ethanol as the elution solvent. Radiochemical purity was determined by radio-TLC or radio-HPLC. The ethanol was evaporated and the activity was reconstituted in phosphate-buffered saline and passed through a 0.22- $\mu\text{m}$  Millipore filter into a sterile multidose vial for in vitro and animal experiments.

### In Vitro Receptor-Binding Studies

In vitro GRPR-binding affinities and specificities of the DOTA-[Lys<sup>3</sup>]BBN conjugate were assessed via displacement cell-binding assays using  $^{125}\text{I}$ -[Tyr<sup>4</sup>]BBN (Perkin-Elmer Life Sciences Products, Inc.) as the GRPR-specific radioligand. Experiments were performed on PC-3 (AI) human prostate cancer cells (American Type Culture Collection) by modification of a method previously described (25). Briefly, cells were grown in Ham's F-12K medium supplemented with 10% fetal bovine serum. PC-3 cells were harvested and seeded in 24-well plates at 10<sup>5</sup> cells per well. Twenty-four hours later, the cells were washed twice with binding buffer containing 50 mmol/L *N*-(2-hydroxyethyl)piperazine-*N'*-(2-ethanesulfonic acid), 125 mmol/L NaCl, 7.5 mmol/L KCl, 5.5 mmol/L MgCl<sub>2</sub>, 1 mmol/L ethylene glycol-bis-( $\beta$ -aminoethyl-ester)-*N,N,N',N'*-tetraacetic acid, 2 mg/mL bovine serum albumin, 2 mg/L chymostatin, 100 mg/L soybean trypsin inhibitor, and 50 mg/L bacitracin at pH 7.4 and then incubated for 1 h at 37°C with 20,000 cpm of  $^{125}\text{I}$ -[Tyr<sup>4</sup>]BBN (specific activity, 74 TBq/mmol [2,000 Ci/mmol]) in the presence of increasing concentrations of DOTA-[Lys<sup>3</sup>]BBN conjugate ranging from 0 to 2,000 nmol/L. After incubation, the cells were washed twice with binding buffer and solubilized with 1N NaOH, and activity was measured in a  $\gamma$ -counter (Packard). The 50% inhibitory concentration (IC<sub>50</sub>) value for the displacement binding of  $^{125}\text{I}$ -[Tyr<sup>4</sup>]BBN by DOTA-[Lys<sup>3</sup>]BBN conjugate was calculated by nonlinear regression analysis using the GraphPad Prism computer-fitting program (GraphPad Software, Inc.). Experiments were done twice with triplicate samples.

## Internalization Studies

Internalization of  $^{64}\text{Cu}$ -DOTA-[Lys<sup>3</sup>]BBN was measured by modifying a previously described technique (25). Briefly, PC-3 (AI) cells were incubated in triplicate in 6-well plates with about 200,000 cpm of  $^{64}\text{Cu}$ -labeled tracer with or without an excess of 1  $\mu\text{mol/L}$  BBN for 2 h at 4°C. After the preincubation, cells were washed with ice-cold binding buffer to remove free radioligand and then incubated with previously warmed binding buffer at 37°C for 0, 15, 30, and 120 min for internalization. The percentage of  $^{64}\text{Cu}$  activity trapped in the cells was determined after removing  $^{64}\text{Cu}$  activity bound to the cell surface by washing twice with acid (50 mmol/L glycine and 0.1 mol/L NaCl, pH 2.8). Cells were then solubilized by incubating with 1N NaOH and counted to determine internalized radioligand.

## Biodistribution

Human prostate cancer carcinoma xenografts were induced by subcutaneous injection of  $10^7$  PC-3 (AI) cells to the left front leg and  $10^7$  CWR22 (AD) cells to the right front leg of 4- to 6-wk-old male athymic nude mice (Harlan). Three to 4 wk later, when the tumors reached 0.4- to 0.6-cm diameter, the mice were injected with 370 kBq (10  $\mu\text{Ci}$ ) DOTA-[Lys<sup>3</sup>]BBN intravenously into the tail vein. Mice ( $n = 4$  per time point) were killed by cervical dislocation at different time points after injection. Blood, tumor, and the major organs and tissues were collected, wet weighed, and counted in a  $\gamma$ -counter (Packard). The percentage of injected dose per gram (%ID/g) was determined for each sample. For each mouse, radioactivity of the tissue samples was calibrated against a known aliquot of the injectate. Values are expressed as mean  $\pm$  SD. The receptor-mediated localization of the radiotracers was investigated by determining the biodistribution of radiolabeled peptide in the presence of 1 and 10 mg/kg of BBN at 1 h after injection ( $n = 4$ ).

## microPET Imaging

PET imaging was performed on a microPET R4 rodent model scanner (Concorde Microsystems, Inc.). The scanner has a computer-controlled bed, 10.8-cm transaxial and 8-cm axial field of view (FOV). It has no septa and operates exclusively in 3-dimensional list mode. All raw data were first sorted into 3-dimensional sinograms, followed by Fourier rebinning and 2-dimensional filtered backprojection image reconstruction using a ramp filter with the Nyquist limit (0.5 cycle/voxel) as the cutoff frequency. For PET imaging of prostate cancer-bearing mice, the animals were injected with 14.8 MBq (400  $\mu\text{Ci}$ )  $^{64}\text{Cu}$ -DOTA-[Lys<sup>3</sup>]BBN via the tail vein. Each mouse was then killed at 1 h after injection and placed near the center of the FOV of the microPET, where the highest image resolution and sensitivity are available. Static imaging was performed for 20 min ( $n = 3$ ). For a receptor-blocking experiment, one mouse bearing PC-3 tumor on the right front leg was imaged (20-min static scan at 1 h after administration of 14.8 MBq [400  $\mu\text{Ci}$ ]  $^{64}\text{Cu}$ -DOTA-[Lys<sup>3</sup>]BBN) twice 2 d apart: (a) without coinjection with BBN; and (b) with 10 mg/kg BBN. No attenuation correction was applied to the microPET scans. Instead, the attenuation correction factors were incorporated into the system calibration. In brief, a vial with a volume (30 mL, 5-cm diameter) similar to that of a nude mouse body was filled with a known amount of  $^{64}\text{CuCl}_2$  and scanned for 1 h. The static scan was reconstructed with the filtered backprojection protocol, and the counting rate from the images of the phantom was compared with the known activity concentration to obtain a system calibration factor. With this approach, the uptake index (ROI [kBq/mL]/

injected dose [kBq]  $\times$  100%, where ROI = region of interest) of tissues and of organs of interest was consistent with the %ID/g value obtained from direct tissue sampling after the microPET imaging. The error was within 5%–10%.

## Whole-Body Autoradiography

Autoradiography was performed using a Packard Cyclone Storage Phosphor Screen system and a Bright 5030/WD/MR cryomicrotome (Hacker Instruments). Immediately after microPET scanning, the mice were frozen in a dry ice and isopropyl alcohol bath for 2 min. The bodies were then embedded in a 4% carboxymethyl cellulose (Aldrich) water mixture using a stainless steel and aluminum mold. The mold was placed in the dry ice and isopropyl alcohol bath for 5 min and then into a  $-20^\circ\text{C}$  freezer for 1 h. The walls of the mold were removed, and the frozen block was mounted in the cryomicrotome. The block was cut into 50- $\mu\text{m}$  sections, and desired sections were digitally photographed and captured for autoradiography. The sections were transferred into a chilled autoradiography cassette containing a Super Resolution Screen (Packard) and kept there overnight at  $-20^\circ\text{C}$ . Screens were read with the Packard Cyclone laser scanner. Quantification of autoradiographic images was validated by a direct tissue sampling technique. In brief, 50- $\mu\text{m}$  slices of tumor tissue were cut and exposed to the Super Resolution Screen for 24 h, and the ROIs drawn from the autoradiographs were described as detector light units per  $\text{mm}^2$  and correlated with direct  $\gamma$ -counter assays of the tissue samples scooped out of the frozen block ( $n = 3$ ). A linear relationship between tissue %ID/g and autoradiography image intensity was obtained, and the conversion factor thus obtained was used for autoradiography quantification.

## Statistic Analysis

Data are expressed as mean  $\pm$  SD. One-way ANOVA was used for statistical evaluation. Means were compared using the Student  $t$  test.  $P$  values  $< 0.05$  were considered significant.

## RESULTS

### Synthesis and Radiolabeling

The DOTA-[Lys<sup>3</sup>]BBN conjugate (Fig. 1) was produced in 75% yield after HPLC purification. The retention time of this compound on HPLC was 18.5 min, whereas [Lys<sup>3</sup>]BBN eluted at 19.2 min under the same conditions. Matrix-assisted laser desorption ionization–time of flight mass spectrometry (MALDI-TOF MS):  $m/z = 1,976$  for  $[\text{M}+\text{H}]^+$  ( $\text{C}_{87}\text{H}_{137}\text{N}_{26}\text{O}_{26}\text{S}$ ); 1,998 for  $[\text{M}+\text{Na}]^+$ ; and 2,014 for  $[\text{M}+\text{K}]^+$ .  $^{64}\text{Cu}$ -DOTA-[Lys<sup>3</sup>]BBN was labeled in  $\geq 90\%$  radiochemical yield and  $\geq 98\%$  radiochemical purity and was used immediately for in vitro and in vivo assays. Free  $^{64}\text{Cu}$ -acetate remained at the origin of the radio-TLC plate and the  $R_f$  value of  $^{64}\text{Cu}$ -DOTA-[Lys<sup>3</sup>]BBN was about 0.5. The specific activity of  $^{64}\text{Cu}$ -DOTA-RGD ranged from 15 to 38 GBq/ $\mu\text{mol}$  (400–1,000 Ci/mmol).

### In Vitro Receptor-Binding Assay

The binding affinity of DOTA-[Lys<sup>3</sup>]BBN conjugate for GRPR was tested for AI human prostate cancer PC-3 cells. As seen in Figure 2, the data show a typical sigmoid curve for the displacement of  $^{125}\text{I}$ -[Tyr<sup>4</sup>]BBN from PC-3 cells as a function of increasing concentrations of the DOTA-



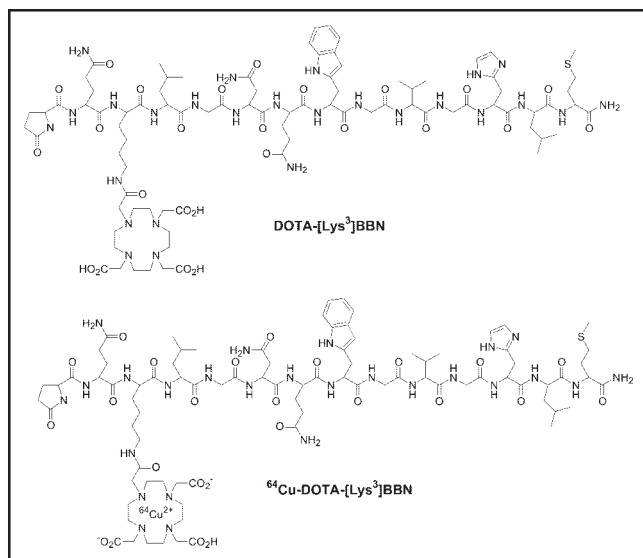


**FIGURE 1.** Schematic structures of DOTA-[Lys<sup>3</sup>]BBN conjugate and <sup>64</sup>Cu-DOTA-[Lys<sup>3</sup>]BBN.

[Lys<sup>3</sup>]BBN conjugate. The IC<sub>50</sub> value was determined to be  $2.2 \pm 0.5$  nmol/L. In the absence of DOTA-[Lys<sup>3</sup>]BBN competitor, approximately 10% of added [<sup>125</sup>I]-[Tyr<sup>4</sup>]BBN was bound. Only about 1% of added radioligand was bound to the cells in the presence of 1  $\mu$ mol/L of DOTA-[Lys<sup>3</sup>]BBN, suggesting that 90% of bound [<sup>125</sup>I]-[Tyr<sup>4</sup>]BBN was GRPR specific.

The internalization of <sup>64</sup>Cu-DOTA-[Lys<sup>3</sup>]BBN into PC-3 cells is illustrated in Figure 3. The rate of internalization was time and temperature dependent. At 4°C, cell surface binding occurred but internalization was minimal (<10%). Incubation at 37°C showed a rapid internalization rate, with  $65\% \pm 10\%$  of radioactivity internalized by 30 min.

#### Biodistribution Studies

A summary of the biodistribution data for <sup>64</sup>Cu-DOTA-[Lys<sup>3</sup>]BBN in PC-3 and CWR22 tumor-bearing mice is

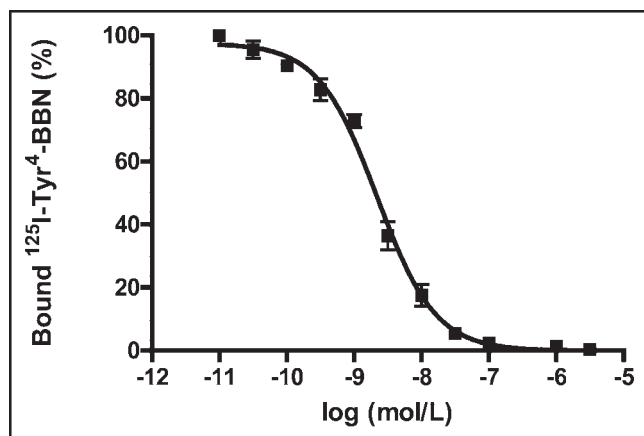


**FIGURE 2.** Inhibition of [<sup>125</sup>I]-[Tyr<sup>3</sup>]BBN binding to GRPR on human prostate cancer cell line PC-3 by DOTA-[Lys<sup>3</sup>]BBN conjugate (IC<sub>50</sub> =  $2.2 \pm 0.5$  nmol/L). Results expressed as percentage of binding are mean  $\pm$  SD of 2 experiments in triplicate.

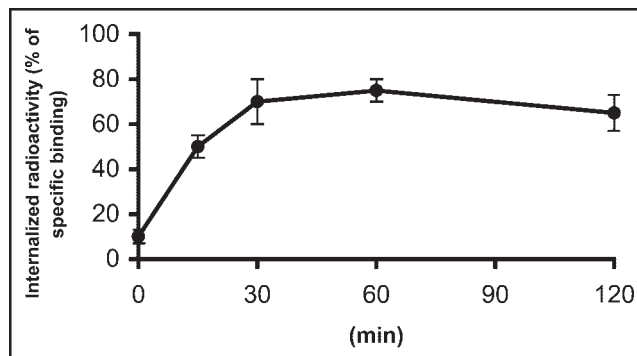


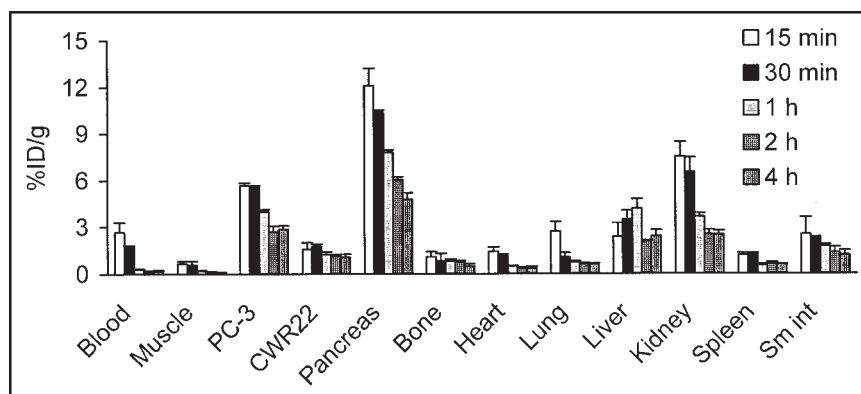
**FIGURE 3.** Time-dependent internalization of <sup>64</sup>Cu-DOTA-[Lys<sup>3</sup>]BBN by PC-3 prostate cancer cells incubated at 37°C during 2 h. Cells were preincubated for 2 h at 4°C. Data are mean  $\pm$  SD of percentage of acid-resistant (internalized) radioactivity in cells (2 experiments in triplicate).

shown in Figure 4. This radiotracer had a rapid blood clearance, with only  $0.30 \pm 0.04$  %ID/g remaining in the circulation at 1 h followed by a further decrease at 2 and 4-h time points. Tumor-to-blood ratios at 1 h were  $13.1 \pm 2.3$  and  $4.1 \pm 1.3$  for PC-3 and CWR22 tumors, respectively. Liver uptake reached maximum at 1 h ( $4.18 \pm 0.63$  %ID/g) and declined to  $2.09 \pm 0.5$  %ID/g at 2 h after injection. The rapid decrease of activity accumulation in the kidneys suggests a predominant renal clearance pathway of this radiotracer. A significant uptake of <sup>64</sup>Cu-DOTA-[Lys<sup>3</sup>]BBN in the GRPR-bearing pancreas was observed ( $10.4 \pm 0.14$  %ID/g at 30 min after injection and  $6.08 \pm 0.18$  %ID/g after 2 h). Our results indicated GRPR-specific uptake in PC-3 tumor and pancreas (Fig. 5), which was confirmed by the receptor-blocking study at the 1-h time point, as the uptake in these tissues was effectively inhibited by coinjection of 10 mg/kg BBN ( $7.83 \pm 0.52$  %ID/g vs.  $0.52 \pm 0.05$  %ID/g for pancreas,  $P < 0.001$ ;  $3.97 \pm 0.15$  %ID/g vs.  $1.35 \pm 0.24$  %ID/g for PC-3 tumor,  $P < 0.001$ ). Coinjection of 1 mg/kg BBN resulted in partial inhibition of activity accumulation in PC-3 tumor ( $2.08 \pm 0.35$  %ID/g) and pancreas ( $2.75 \pm 0.43$  %ID/g). Activity accumulation in the AD CWR22 tumor was not affected by the administration of BBN. No significant changes of uptake in other normal organs were seen except for the kidneys, which had increased uptake in the blocked versus the control mice ( $P < 0.01$ ), presumably due to decreased specific binding in tissues.

#### microPET and Autoradiographic Imaging

The localization of <sup>64</sup>Cu-DOTA-[Lys<sup>3</sup>]BBN in PC-3 and CWR22 tumor-bearing mice as determined by microPET imaging followed by whole-body autoradiography is depicted in Figure 6. On the left is a coronal image of a tumor-bearing mouse 1 h after administration of 14.8 MBq (400  $\mu$ Ci) <sup>64</sup>Cu-DOTA-[Lys<sup>3</sup>]BBN. The microPET image is concordant with a whole-body autoradiographic section seen on the right. Both PC-3 (left) and CWR22 (right) tumors were visible with clear contrast from the adjacent background. Prominent uptake was also observed in the

**FIGURE 4.** Biodistribution of  $^{64}\text{Cu}$ -DOTA-[Lys<sup>3</sup>]BBN in male athymic nude mice bearing subcutaneous PC-3 (AI) and CWR22 (AD) tumors. Mice were intravenously injected with 370 kBq (10  $\mu\text{Ci}$ ) of radioligand and killed at 15 min, 30 min, 1 h, 2 h, and 4 h. Data are presented as mean %ID/g  $\pm$  SD ( $n = 4$ ). Sm int = small intestine.



liver and kidneys, and clearance of the activity through the urinary bladder is evident. Uptake indices at 1 h derived from microPET (tail vein injection of 14.8 MBq [400  $\mu\text{Ci}$ ] activity) and quantitative autoradiography (QAR) are compared with data obtained from direct tissue sampling (tail vein injection of 370 kBq [10  $\mu\text{Ci}$ ] activity) in Figure 7. The results from microPET ROI analysis agreed with the results obtained from autoradiographic quantification for the organs and tissues examined. It is evident that PC-3 tumor and pancreas uptake obtained from microPET and QAR were significantly lower than those obtained from the direct biodistribution measurement. Figure 8 shows transaxial microPET images of a PC-3 tumor-bearing nude mouse, 1 h after administration of  $^{64}\text{Cu}$ -DOTA-[Lys<sup>3</sup>]BBN, with and without coinjection of 10 mg/kg BBN. There is a clear visualization of the PC-3 tumor in the animal on the left without the presence of competitor. Conversely, the same mouse that received a blocking dose of BBN showed reduced tracer localization in the tumor.

## DISCUSSION

This study showed that suitably labeled BBN analogs can be used to image both AI and AD prostate cancer in pre-

clinical animal models. In particular, this study demonstrated that AI PC-3 but not AD CWR22 prostate cancer tumor has GRPR-specific activity accumulation.

The overexpression of peptide receptors in human tumors is of considerable interest for tumor imaging and therapy. Because of their small size, peptides have faster blood clearance and higher target-to-background ratios compared with those of macromolecular compounds. Radiolabeled receptor-binding peptides have recently emerged as a new class of radiopharmaceuticals. Various peptides have been used for tumor scintigraphy. For example, somatostatin receptors, which are highly expressed in most neuroendocrine tumors, have been targeted successfully for both imaging and therapy with octreotide. The long-term treatment of patients with octreotide has been successful in relieving the symptoms resulting from excessive hormone production by the tumors (28). The use of radiolabeled somatostatin analogs has permitted imaging as well as therapy of neuroendocrine tumors and their metastases in patients (29). Similar targeting strategies have also been applied to vasoactive intestinal peptide receptors in epithelial tumors (30) and cholecystikinin-B receptors in medullary thyroid car-

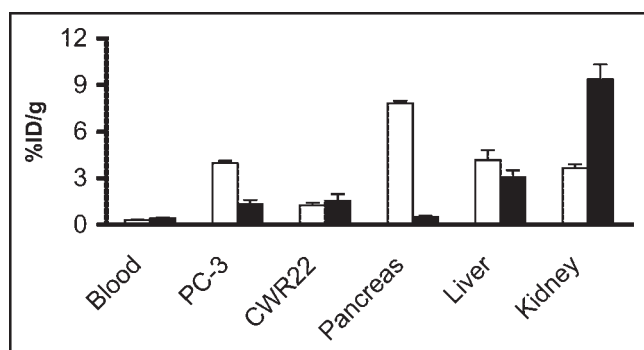


**FIGURE 5.** Receptor-blocking study: biodistribution of  $^{64}\text{Cu}$ -DOTA-[Lys<sup>3</sup>]BBN at 1-h time point without (white bars) and with (black bars) coinjection of 200  $\mu\text{g}$  of BBN to determine GRPR-specific binding. Significant inhibition of activity accumulation in PC-3 tumor ( $P < 0.001$ ) and pancreas ( $P < 0.001$ ) was observed. Data are presented as mean %ID/g  $\pm$  SD in reference to total injected dose of radiotracer ( $n = 4$  for each group).

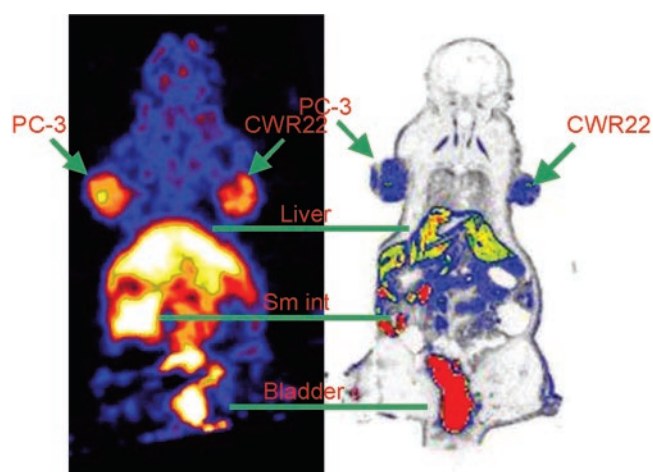


**FIGURE 6.** (Left) Coronal microPET image of tumor-bearing mouse (PC-3 on left shoulder and CWR22 on right shoulder) 1 h after administration of  $^{64}\text{Cu}$ -DOTA-[Lys<sup>3</sup>]BBN. (Right) Digital autoradiograph of section containing tumors.

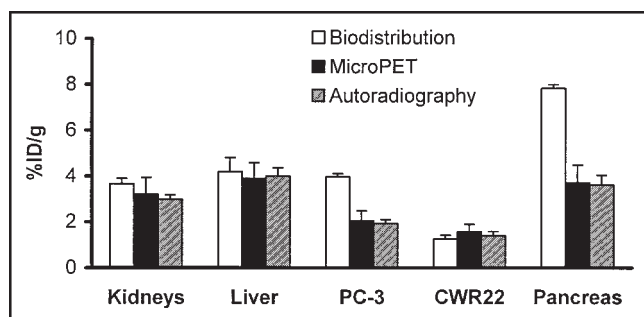


**FIGURE 7.** Kidney, liver, PC-3 tumor, and CWR22 tumor uptake comparison as obtained from traditional biodistribution ( $n = 4$ ), microPET ( $n = 3$ ), and autoradiographic quantification ( $n = 3$ ). Quantification of microPET and autoradiography revealed similar activity accumulation in both PC-3 tumor and pancreas, which were both lower than those obtained from biodistribution study.

cinomas and small cell lung cancers (31). Recently, we and other groups have labeled cyclic RGD peptides with various radionuclides for imaging of tumor angiogenesis (32,33). Overexpression of the GRPR in a variety of neoplasias, such as breast, prostate, pancreatic, and small cell lung cancers, was prompted by the development of  $\gamma$ -emitting or positron-emitting radionuclide-labeled GRP analogs for SPECT (20–25,34) and PET (27) imaging of GRPR-positive tumors.

Since the native BBN peptide has a pyroglutamic acid at the N-terminus and an amidated methionine at the C-terminus, further modification and radiolabeling of this peptide with metallic radionuclides is not possible. Efforts have been made to design derivatized BBN analogs for binding and pharmacokinetic studies. Because BBN agonists are generally preferable to BBN antagonists for receptor-specific internalization, most BBN analogs with an amidated C-terminus that have been developed are agonists. Because the C-terminus is directly involved in the specific binding interaction with the GRPR, the truncated C-terminal heptapeptide sequence Trp-Ala-Val-Gly-His-Leu-Met (BBN(8–14)) must be maintained or minimally substituted. Several strategies have been applied to develop radiometallated BBN-analogous conjugates. For example, the N-terminal Glp of BBN has been replaced by Pro and subsequently conjugated with DOTA and diethylenetriaminepentaacetic acid (DTPA) for  $^{111}\text{In}$  labeling (35,36); Arg<sup>3</sup> was substituted with Lys<sup>3</sup> and a  $\text{N}_2\text{S}_2$  ligand was attached to the Lys side chain  $\epsilon$ -amino group for  $^{99\text{m}}\text{Tc}$  labeling (22) or DOTA and DTPA were attached to Lys<sup>3</sup> of [Lys<sup>3</sup>,Tyr<sup>4</sup>]BBN for  $^{111}\text{In}$  labeling (35). Most of the studies reported to date used a C-terminal amidated BBN(8–14) in which radiometal chelate was linked to the truncated small peptide (37,38) for  $^{99\text{m}}\text{Tc}$  labeling[b]. Recently, Rogers et al. (27) reported  $^{64}\text{Cu}$ -labeled, DOTA-conjugated, Aoc linker-modified BBN(7–14) for microPET imaging of subcutaneous PC-3 tumor models. The strategy used in our laboratory has focused primarily on modification of the Lys<sup>3</sup> residue of [Lys<sup>3</sup>]BBN with various linkers and chelators for diagnostic

and therapeutic applications. This study reports  $^{64}\text{Cu}$ -labeled DOTA-[Lys<sup>3</sup>]BBN for microPET imaging of both AI and AD tumor models.

In contrast to many other investigators who tried to conjugate DOTA chelator to peptides via solid-phase synthesis using DOTA-tris(*t*-butyl ester) followed by TFA cleavage and deprotection, we found that the incorporation yield of tri-*t*-butyl ester-protected DOTA to fully protected peptides fixed on resin was low due to steric hindrance of the bulky protecting groups. Purification of the peptide conjugates was difficult due to the fact that DOTA-peptide conjugates usually had a retention time similar to those of the parent peptides. We also found it more convenient to prepare DOTA-peptide conjugates in buffer solutions via *in situ* activation of DOTA. The retention time of DOTA-[Lys<sup>3</sup>]BBN is different from that of [Lys<sup>3</sup>]BBN by <1 min under the HPLC condition in this study. However, the use of an excess amount of DOTA for conjugation resulted in almost complete conversion of [Lys<sup>3</sup>]BBN to DOTA-[Lys<sup>3</sup>]BBN. The radiolabeling of DOTA-[Lys<sup>3</sup>]BBN with  $^{64}\text{Cu}$  was performed with high yield. Unreacted  $^{64}\text{Cu}$  was easily removed by simple  $\text{C}_{18}$  cartridge elution.

DOTA-[Lys<sup>3</sup>]BBN had high affinity for the GRPR ( $\text{IC}_{50} = 2.2 \pm 0.5 \text{ nmol/L}$ ; Fig. 2) similar to that of BBN (1.5 nmol/L) (25). This study agrees with the findings by Baidoo et al. (22) that modification of the Lys<sup>3</sup>  $\epsilon$ -amino group has little effect on the receptor-binding characteristics of the peptide.  $^{64}\text{Cu}$ -Labeled DOTA-[Lys<sup>3</sup>]BBN was rapidly internalized by PC-3 cells, consistent with the expected agonistic behavior of this radiotracer against GRPR. Maximum internalization and retention of the radioactivity by tumor cells is needed for diagnostic or therapeutic efficacy of radiopharmaceuticals. There was limited efflux of  $^{64}\text{Cu}$  activity from the PC-3 cells within the period of investigation (2 h), presumably due to residualization of  $^{64}\text{Cu}$  from GRPR-mediated entrapment of the tracer in lysosomes (39,40) and subsequent degradation by lysosomal proteases. Similar results have been obtained with other radiolabeled BBN analogs.

Biodistribution studies were performed on both PC-3 (AI) and CWR22 (AD) tumor-bearing mice. It has been



**FIGURE 8.** Transaxial microPET images of athymic nude mouse bearing PC-3 tumor on right shoulder 1 h after tail vein injection of 14.8 MBq (400  $\mu\text{Ci}$ )  $^{64}\text{Cu}$ -DOTA-[Lys<sup>3</sup>]BBN in absence (control) and presence (block) of coinjected blocking dose of BBN (10 mg/kg). Arrows indicate location of tumors.



reported that AI tumor cells express GRPRs at significantly higher levels than do AD tumor cells (16). In the current study, activity accumulation from  $^{64}\text{Cu}$ -DOTA-[Lys<sup>3</sup>]BBN by AI PC-3 tumors was significantly higher than by AD CWR22 tumors. It is interesting to note that receptor blocking did not reduce the uptake in CWR22 tumor, whereas the activity in GRPR-positive PC-3 tumor and pancreas were effectively inhibited. Fast blood clearance of radiotracer after 30 min following administration might have been due to little binding of the degradation metabolites to plasma proteins. This is very different from the in vivo behavior of  $^{64}\text{Cu}$ -DOTA-Aoc-BBN(7–14) (27), which exhibited persistent blood retention up to 24 h after injection and higher normal tissue uptake than that reported in this and other studies. A high degree of plasma protein binding of the relatively lipophilic Aoc linker as well as transchelation of  $\text{Cu}^{2+}$  to albumin and superoxide dismutase may have caused the unfavorably high liver activity accumulation. Smith et al. (38) also reported that a long aliphatic linker is responsible for prolonged retention in blood and decreased pancreatic uptake.

Although  $^{99\text{m}}\text{Tc}$ -labeled GRP analogs have receptor-specific tumor activity accumulation, the absolute tumor uptake is rather low ( $<1\%$  ID/g at 1 h after injection).  $^{64}\text{Cu}$ -Labeled BBN analogs reported here and by Rogers et al. (27) gave much higher tumor uptake and more persistent tumor retention. Further investigations are needed to fully understand the effect of radiochelate characteristics, linker properties, and peptide sequences on tumor-targeting ability and excretion kinetics. As opposed to  $^{64}\text{Cu}$ -DOTA-Aoc-BBN(7–14), which had both hepatobiliary and renal excretion pathways,  $^{64}\text{Cu}$ -DOTA-[Lys<sup>3</sup>]BBN was excreted rapidly via the renal route. This suggests that insertion of a rather hydrophobic aliphatic acid linker to separate the radiolabel from the receptor-targeting peptide moiety is probably not beneficial for optimization of such radioligands.

microPET imaging of  $^{64}\text{Cu}$ -DOTA-[Lys<sup>3</sup>]BBN in mice bearing both AI PC-3 and AD CWR22 tumors 1 h after injection of radioactivity revealed a high tumor-to-background ratio for both tumor types (Fig. 6). The uptake indices found with microPET and QAR for PC-3 tumor and pancreas were significantly lower than those obtained from direct tissue sampling (Fig. 7). Assuming the specific activity of the radiotracer was  $18.5\text{ GBq}/\mu\text{mol}$  ( $500\text{ mCi}/\mu\text{mol}$ ) at the time of tail vein injection, the injection administered for microPET imaging contained about  $2\text{ }\mu\text{g}$  BBN peptide ( $14.8\text{ MBq}$  [ $400\text{ }\mu\text{Ci}$ ]), whereas the amount of activity administered for the biodistribution experiment contained only  $50\text{ ng}$  BBN peptide ( $370\text{ kBq}$  [ $10\text{ }\mu\text{Ci}$ ]). It is possible that partial self-inhibition of receptor-specific uptake in PC-3 tumor, pancreas, and other tissues that express the GRPR occurred during the imaging studies. Conversely, the inability to inhibit CWR22 tumor activity accumulation in the imaging study is consistent with the known low GRPR expression in AD tumors such as CWR22 (16).

We anticipate that quantitative imaging with microPET in living animals, based on the overexpression of GRPR in invasive prostate cancer, could potentially be translated into clinical settings to detect AI prostate cancer. Successful targeting of this molecular pathway would have diagnostic as well as potential radio- and chemotherapeutic implications: the ability to document GRPR density and the appropriate selection of patients entering clinical trials for anti-GRPR treatment. PET imaging of prostate cancer with  $^{64}\text{Cu}$ -labeled BBN analogs also will be useful for determining dosimetry and tumor response to the same ligand labeled with therapeutic amounts of  $^{67}\text{Cu}$  for internal radiotherapy.

## CONCLUSION

[Lys<sup>3</sup>]BBN, when conjugated with a macrocyclic DOTA-chelating group and radiolabeled with the positron-emitting radionuclide  $^{64}\text{Cu}$ , exhibits high GRPR-binding affinity and specificity and rapid internalization in AI PC-3 prostate cancer cells. Specific localization of  $^{64}\text{Cu}$ -DOTA-[Lys<sup>3</sup>]BBN to PC-3 tumor and GRPR-positive tissues was confirmed by biodistribution, microPET imaging, and autoradiographic imaging studies. Reduced tumor uptake in PC-3 tumor but not CWR22 tumor in high-dose microPET and autoradiography studies compared with low-dose biodistribution studies further illustrates high-affinity and low-capacity characteristics of the GRPR in AI tumors. The activity accumulation in CWR22 tumor is attributed to nonspecific uptake. Further studies to evaluate the metabolic stability and optimization of the radiotracers for prolonged tumor retention and improved in vivo kinetics are necessary.

## ACKNOWLEDGMENTS

This work was funded by the Department of Defense Prostate Cancer Research Program DAMD17-03-1-0143 and National Institutes of Health grant P20 CA86532. Production of  $^{64}\text{Cu}$  at Washington University School of Medicine was supported by National Cancer Institute grant R24 CA86307.

## REFERENCES

- Effert PJ, Bares R, Handt S, Wolff JM, Bull U, Jakse G. Metabolic imaging of untreated prostate cancer by positron emission tomography with  $^{18}\text{F}$ -labeled deoxyglucose. *J Urol*. 1996;155:994–998.
- Liu JJ, Zafar MB, Lai YH, Segall GM, Terris MK. Fluorodeoxyglucose positron emission tomography studies in diagnosis and staging of clinically organ-confined prostate cancer. *Urology*. 2001;57:108–111.
- Hara T, Kosaka N, Kishi H. PET imaging of prostate cancer using carbon-11-choline. *J Nucl Med*. 1998;39:990–995.
- Kotzerke J, Prang J, Neumaier B, et al. Experience with carbon-11 choline positron emission tomography in prostate carcinoma. *Eur J Nucl Med*. 2000;27:1415–1419.
- Price DT, Coleman RE, Liao RP, Robertson CN, Polascik TJ, DeGrado TR. Comparison of [ $^{18}\text{F}$ ]fluorocholine and [ $^{18}\text{F}$ ]fluorodeoxyglucose for positron emission tomography of androgen dependent and androgen independent prostate cancer. *J Urol*. 2002;168:273–280.
- DeGrado TR, Baldwin SW, Wang S, et al. Synthesis and evaluation of  $^{18}\text{F}$ -labeled choline analogs as oncologic PET tracers. *J Nucl Med*. 2001;42:1805–1814.

7. DeGrado TR, Coleman RE, Wang S, et al. Synthesis and evaluation of  $^{18}\text{F}$ -labeled choline as an oncologic tracer for positron emission tomography: initial findings in prostate cancer. *Cancer Res.* 2001;61:110–117.
8. Hara T, Kosaka N, Kishi H. Development of  $^{18}\text{F}$ -fluoroethylcholine for cancer imaging with PET: synthesis, biochemistry, and prostate cancer imaging. *J Nucl Med.* 2002;43:187–199.
9. Kotzerke J, Volkmer BG, Neumaier B, Gschwend JE, Hautmann RE, Reske SN. Carbon-11 acetate positron emission tomography can detect local recurrence of prostate cancer. *Eur J Nucl Med Mol Imaging.* 2002;29:1380–1384.
10. Kato T, Tsukamoto E, Kuge Y, et al. Accumulation of [ $^{11}\text{C}$ ]acetate in normal prostate and benign prostatic hyperplasia: comparison with prostate cancer. *Eur J Nucl Med Mol Imaging.* 2002;29:1492–1495.
11. Oyama N, Akino H, Kanamaru H, et al.  $^{11}\text{C}$ -Acetate PET imaging of prostate cancer. *J Nucl Med.* 2002;43:181–186.
12. Oyama N, Miller TR, Dehdashti F, et al.  $^{11}\text{C}$ -Acetate PET imaging of prostate cancer: detection of recurrent disease at PSA relapse. *J Nucl Med.* 2003;44:549–555.
13. Bonasera TA, O'Neil JP, Xu M, et al. Preclinical evaluation of fluorine-18-labeled androgen receptor ligands in baboons. *J Nucl Med.* 1996;37:1009–1015.
14. Markwalder R, Reubi JC. Gastrin-releasing peptide receptors in the human prostate: relation to neoplastic transformation. *Cancer Res.* 1999;59:1152–1159.
15. Sun B, Halmos G, Schally AV, Wang X, Martinez M. Presence of receptors for bombesin/gastrin-releasing peptide and mRNA for three receptor subtypes in human prostate cancers. *Prostate.* 2000;42:295–303.
16. Reile H, Armatas PE, Schally AV. Characterization of high-affinity receptors for bombesin/gastrin releasing peptide on the human prostate cancer cell lines PC-3 and DU-145: internalization of receptor bound  $^{125}\text{I}$ -(Tyr $^4$ ) bombesin by tumor cells. *Prostate.* 1994;25:29–38.
17. Jongsma J, Oomen MH, Noordzij MA, et al. Androgen-independent growth is induced by neuropeptides in human prostate cancer cell lines. *Prostate.* 2000;42:34–44.
18. Szepeshazi K, Halmos G, Schally AV, et al. Growth inhibition of experimental pancreatic cancers and sustained reduction in epidermal growth factor receptors during therapy with hormonal peptide analogs. *J Cancer Res Clin Oncol.* 1999;125:444–452.
19. Schally AV, Comaru-Schally AM, Plonowski A, Nagy A, Halmos G, Rekasi Z. Peptide analogs in the therapy of prostate cancer. *Prostate.* 2000;45:158–166.
20. Van de Wiele C, Dumont F, Dierckx RA, et al. Biodistribution and dosimetry of  $^{99\text{m}}\text{Tc}$ -RP527, a gastrin-releasing peptide (GRP) agonist for the visualization of GRP receptor-expressing malignancies. *J Nucl Med.* 2001;42:1722–1727.
21. Van de Wiele C, Dumont F, Vanden Broecke R, et al. Technetium-99m RP527, a GRP analogue for visualisation of GRP receptor-expressing malignancies: a feasibility study. *Eur J Nucl Med.* 2000;27:1694–1699.
22. Baidoo KE, Lin KS, Zhan Y, Finley P, Scheffel U, Wagner HN Jr. Design, synthesis, and initial evaluation of high-affinity technetium bombesin analogues. *Bioconjug Chem.* 1998;9:218–225.
23. Karra SR, Schibli R, Gali H, et al.  $^{99\text{m}}\text{Tc}$ -Labeling and in vivo studies of a bombesin analogue with a novel water-soluble dithiadiphosphine-based bifunctional chelating agent. *Bioconjug Chem.* 1999;10:254–260.
24. La Bella R, Garcia-Garayoa E, Langer M, Blauenstein P, Beck-Sickinger AG, Schubiger PA. In vitro and in vivo evaluation of a  $^{99\text{m}}\text{Tc}$ (I)-labeled bombesin analogue for imaging of gastrin releasing peptide receptor-positive tumors. *Nucl Med Biol.* 2002;29:553–560.
25. La Bella R, Garcia-Garayoa E, Bahler M, et al. A  $^{99\text{m}}\text{Tc}$ (I)-postlabeled high affinity bombesin analogue as a potential tumor imaging agent. *Bioconjug Chem.* 2002;13:599–604.
26. Wu AM, Yazaki PJ, Tsai S, et al. High-resolution microPET imaging of carcinoembryonic antigen-positive xenografts by using a copper-64-labeled engineered antibody fragment. *Proc Natl Acad Sci USA.* 2000;97:8495–8500.
27. Rogers BE, Bigott HM, McCarthy DW, et al. MicroPET imaging of a gastrin-releasing peptide receptor-positive tumor in a mouse model of human prostate cancer using a  $^{64}\text{Cu}$ -labeled bombesin analogue. *Bioconjug Chem.* 2003;14:756–763.
28. Lamberts SW, Krenning EP, Reubi JC. The role of somatostatin and its analogs in the diagnosis and treatment of tumors. *Endocr Rev.* 1991;12:450–482.
29. Breeman WA, de Jong M, Kwekkeboom DJ, et al. Somatostatin receptor-mediated imaging and therapy: basic science, current knowledge, limitations and future perspectives. *Eur J Nucl Med.* 2001;28:1421–1429.
30. Virgolini I, Raderer M, Kurtaran A, et al. Vasoactive intestinal peptide-receptor imaging for the localization of intestinal adenocarcinomas and endocrine tumors. *N Engl J Med.* 1994;331:1116–1121.
31. Behr TM, Jenner N, Radetzky S, et al. Targeting of cholecystokinin-B/gastrin receptors in vivo: preclinical and initial clinical evaluation of the diagnostic and therapeutic potential of radiolabelled gastrin. *Eur J Nucl Med.* 1998;25:424–430.
32. Chen X, Park R, Shahinian AH, et al.  $^{18}\text{F}$ -Labeled RGD peptide: initial evaluation for imaging brain tumor angiogenesis. *Nucl Med Biol.* 2004;31:179–189.
33. Haubner R, Wester HJ, Weber WA, et al. Noninvasive imaging of  $\alpha_v\beta_3$  integrin expression using  $^{18}\text{F}$ -labeled RGD-containing glycopeptide and positron emission tomography. *Cancer Res.* 2001;61:1781–1785.
34. Smith CJ, Volkert WA, Hoffman TJ. Gastrin releasing peptide (GRP) receptor targeted radiopharmaceuticals: a concise update. *Nucl Med Biol.* 2003;30:861–868.
35. Breeman WA, de Jong M, Erion JL, et al. Preclinical comparison of  $^{111}\text{In}$ -labeled DTPA- or DOTA-bombesin analogs for receptor-targeted scintigraphy and radionuclide therapy. *J Nucl Med.* 2002;43:1650–1656.
36. Breeman WA, De Jong M, Bernard BF, et al. Pre-clinical evaluation of [ $^{111}\text{In}$ -DTPA-Pro $^1$ ,Tyr $^4$ ]bombesin, a new radioligand for bombesin-receptor scintigraphy. *Int J Cancer.* 1999;83:657–663.
37. Hoffman TJ, Gali H, Smith CJ, et al. Novel series of  $^{111}\text{In}$ -labeled bombesin analogs as potential radiopharmaceuticals for specific targeting of gastrin-releasing peptide receptors expressed on human prostate cancer cells. *J Nucl Med.* 2003;44:823–831.
38. Smith CJ, Gali H, Sieckman GL, Higginbotham C, Volkert WA, Hoffman TJ. Radiochemical investigations of  $^{99\text{m}}\text{Tc}$ -N $_3$ S-X-BBN[7-14]NH $_2$ : an in vitro/in vivo structure-activity relationship study where X = 0-, 3-, 5-, 8-, and 11-carbon tethering moieties. *Bioconjug Chem.* 2003;14:93–102.
39. Slice LW, Yee HF Jr, Walsh JH. Visualization of internalization and recycling of the gastrin releasing peptide receptor-green fluorescent protein chimera expressed in epithelial cells. *Recept Channels.* 1998;6:201–212.
40. Grady EF, Slice LW, Brant WO, Walsh JH, Payan DG, Bunnett NW. Direct observation of endocytosis of gastrin releasing peptide and its receptor. *J Biol Chem.* 1995;270:4603–4611.



# Comparative in vitro and in vivo evaluation of two $^{64}\text{Cu}$ -labeled bombesin analogs in a mouse model of human prostate adenocarcinoma

Yi-Shan Yang, Xianzhong Zhang, Zhengming Xiong, Xiaoyuan Chen\*

Department of Radiology and Bio-X Program, The Molecular Imaging Program at Stanford (MIPS), Stanford University School of Medicine, Stanford, CA 94305-5484, USA

Received 9 October 2005; received in revised form 30 November 2005; accepted 4 December 2005

## Abstract

Bombesin (BBN), an analog of human gastrin-releasing peptide (GRP), binds to the GRP receptor (GRPR) with high affinity and specificity. Overexpression of GRPR has been discovered in mostly androgen-independent human prostate tissues and, thus, provides a potential target for prostate cancer diagnosis and therapy. We have previously demonstrated the feasibility of the positron emission tomography (PET) imaging using  $^{64}\text{Cu}$ -1,4,7,10-tetraazadodecane- $\text{N},\text{N}',\text{N}'',\text{N}'''$ -tetraacetic acid (DOTA)-[Lys<sup>3</sup>]BBN to detect GRPR-positive prostate cancer. In this study, we compared the receptor affinity, metabolic stability, tumor-targeting efficacy, and pharmacokinetics of a truncated BBN analog  $^{64}\text{Cu}$ -DOTA-Aca-BBN(7-14) with  $^{64}\text{Cu}$ -DOTA-[Lys<sup>3</sup>]BBN. Binding of each DOTA conjugate to GRPR on PC-3 and 22Rv1 prostate cancer cells was evaluated with competitive binding assay using  $^{125}\text{I}$ -[Tyr<sup>4</sup>]BBN as radioligand. In vivo pharmacokinetics was determined on male nude mice subcutaneously implanted with PC-3 cells. Dynamic microPET imaging was performed to evaluate the systemic distribution of the tracers. Metabolic stability of the tracers in blood, urine, tumor, liver and kidney was studied using high-performance liquid chromatography. The results showed that  $^{125}\text{I}$ -[Tyr<sup>4</sup>]BBN has a  $K_d$  of  $14.8 \pm 0.4$  nM against PC-3 cells, and the receptor concentration on PC-3 cell surface is approximately  $2.7 \pm 0.1 \times 10^6$  receptors per cell. The 50% inhibitory concentration value for DOTA-Aca-BBN(7-14) is  $18.4 \pm 0.2$  nM, and that for DOTA-[Lys<sup>3</sup>]BBN is  $2.2 \pm 0.5$  nM. DOTA-[Lys<sup>3</sup>]BBN shows a better tumor contrast and absolute tumor activity accumulation compared to DOTA-Aca-BBN(7-14). Studies on metabolic stability for both tracers on organ homogenates showed that  $^{64}\text{Cu}$ -DOTA-[Lys<sup>3</sup>]BBN is relatively stable. This study demonstrated that both tracers are suitable for targeted PET imaging to detect the expression of GRPR in prostate cancer, while  $^{64}\text{Cu}$ -DOTA-[Lys<sup>3</sup>]BBN may have a better potential for clinical translation.

© 2006 Elsevier Inc. All rights reserved.

**Keywords:** GRP Receptor; Bombesin;  $^{64}\text{Cu}$ ; MicroPET; Prostate Cancer

## 1. Introduction

Prostate cancer is the most diagnosed malignant growth in men and is the second leading cause of male cancer deaths in the majority of Western countries [1]. As life expectancy increases, so will the incidence of this disease, creating what will become an epidemic male health problem. Imaging evaluation of prostate cancer continues to be challenging [2]. As oncology departs from nonspecific diagnosis and treatment toward individualized molecular therapy, accurate knowledge of the molecular features of prostate cancer becomes even more crucial in order to tailor the treatment plan appropriately. The cancer usually starts

from an androgen-dependent (AD) lesion in the prostate gland. However, during androgen ablation therapy, androgen-independent (AI) tumor cells eventually emerge, leading to clinical relapse [3]. There is currently no effective treatment available for AI prostate cancer. Factors involved in the transition of prostate cancer cells from AD to AI are not well established. The interaction between gastrin-releasing peptide (GRP)/bombesin (BBN) and GRP receptor (GRPR) as an autocrine tumor growth stimulating pathway has been repeatedly reported in the pathogenesis of a large number of mammalian carcinomas, among them are thyroid [4], pancreatic [5], gastric [6], colorectal [7], breast [8], prostatic [9], duodenal carcinomas [10] and gastrinomas [11]. It also has been established that GRPR is overexpressed in resected human biopsy specimen of these lesions, as compared to normal surrounding tissue [12]. GRP

\* Corresponding author. Tel.: +1 650 725 0950; fax: +1 650 736 7925  
E-mail address: [shawchen@stanford.edu](mailto:shawchen@stanford.edu) (X. Chen).

promotes the growth and invasiveness of prostate cancer in vitro [13], and its secretion in vivo by endocrine cells is thought to be partially responsible for AI progression of the disease [14] by transactivation and up-regulation of epidermal growth factor receptors [15,16].

Cancer treatment with GRPR antagonists in either monotherapy or combination therapy, radiotherapy with radiolabeled GRP analogs and use of GRPR-targeted delivery of toxins may prove to be new and effective therapeutic approaches [17,18]. The ability to visualize and quantify GRPR expression level noninvasively will be critical for GRPR targeted therapies, as in vivo GRPR imaging will allow early tumor diagnosis and patient stratification based upon GRPR expression and predict response to this GRPR-targeted treatment. Several BBN analogs have been conjugated with different chelating agents and labeled with various radiometals for diagnosis and treatment of GRPR-positive lesions [19–24]. Most of the studies assume that the truncated sequence BBN(7–14) was sufficient for the specific binding interaction with the GRPR and metabolically stable enough for in vivo applications. Technetium-99m RP527, which contains a tripeptide N3S chelator for  $^{99m}\text{Tc(V)O}$  complexation, a gly-5Ava linker and BBN(7–14) has been investigated in GRPR-positive tumors in patients, exhibits favorable dosimetry, specific tumor localization and good imaging characteristics [25,26].

Positron emission tomography (PET) has the advantages over single photon emission computed tomography in two aspects. The higher sensitivity is particularly valuable for detecting the fewest possible cells per unit volume with the least amount of radioactivity. The spatial/temporal resolution of PET is also significantly higher, allowing dynamic scans and small lesion detection. However, very few PET studies for visualization and quantification of GRPR expression have been reported to date [27–30].

Copper-64 ( $t_{1/2}$ , 12.7 h; 39%  $\beta^-$  [0.58 MeV]; 17.4%  $\beta^+$  [0.65 MeV]; 43.6% electron capture) [31] has a modest positron yield and intermediate half-life, providing an adequate flux of annihilation photons to allow imaging of the biodistribution by PET. It also has Auger and energetic beta emissions suitable for effective short-range cell killing, serving as an internally administered therapeutic radionuclide for small to medium tumor masses [32]. Rogers et al. [30] developed a truncated form of a  $^{64}\text{Cu}$ -labeled BBN analogue,  $^{64}\text{Cu}$ -1,4,7,10-tetraazadodecane-N,N',N'',N'''-tetraacetic acid (DOTA)-Aoc-BBN(7–14). The study showed that this truncated BBN peptide with an alkyl linker has high affinity and internalization on GRP-positive cells (Fig. 1A). It also showed successful targeting and accumulation in PC-3 tumor. Alternatively, a poly(ethylene glycol) linker (M.W.=3400) resulted in significantly reduced receptor affinity and lower receptor specific activity accumulation in vivo [33]. We recently reported the synthesis and pharmacologic evaluation of another  $^{64}\text{Cu}$ -labeled BBN analogue, viz.,  $^{64}\text{Cu}$ -DOTA-[Lys<sup>3</sup>]BBN, for

targeting GRPR expression in prostate cancer [29]. In this previously reported study,  $^{125}\text{I}$ -[Tyr<sup>4</sup>]BBN had a 50% inhibitory concentration value of  $2.2 \pm 0.5$  nmol/L for DOTA-[Lys<sup>3</sup>]BBN against PC-3 cells. Internalization of this radioligand to PC-3 cells was temperature- and time-dependent. Radiotracer uptake was higher in AI PC-3 than in AD 22Rv1 tumor. Coinjection of a blocking dose of [Lys<sup>3</sup>]BBN also revealed inhibition of the activity accumulation in PC-3 tumor and pancreas but not in 22Rv1 tumor. In addition, microPET and autoradiographic imaging of  $^{64}\text{Cu}$ -DOTA-[Lys<sup>3</sup>]BBN in athymic nude mice bearing subcutaneous PC-3 and 22Rv1 tumors showed strong tumor-to-background contrast for PC-3 tumor.

However, it is unclear whether the C-terminal fragment or the full-length of the amphibian tetradecapeptide BBN is more suitable for GRPR targeting in vivo. In order to investigate the nature of these two types of BBN analogues, in this study, we continued to characterize  $^{64}\text{Cu}$ -DOTA-[Lys<sup>3</sup>]BBN and extended the methodology to  $^{64}\text{Cu}$ -DOTA-Aca-BBN(7–14), where Aca refers to  $\epsilon$ -aminocaproic acid. For both compounds, in vitro assays, metabolic stability and microPET studies were performed to investigate tumor targeting and in vivo kinetics.

## 2. Materials and methods

### 2.1. Chemical synthesis, identification and characterization

[Lys<sup>3</sup>]BBN and Aca-BBN(7–14) were synthesized using solid-phase Fmoc chemistry by American Peptide (Sunnyvale, CA, USA). Reagent grade of DOTA, Macrocylics, Dallas, TX, USA), 1-ethyl-3-[3-(dimethylamino)propyl]carbodiimide (EDC, Fluka BioChemika, St. Louis, MO, USA) and *N*-hydroxysulfonosuccinimide (SNHS, Fluka BioChemika, St. Louis, MO, USA) were used as received (Fig. 1B). Conjugation of DOTA with [Lys<sup>3</sup>]BBN and Aca-BBN(7–14) followed the standard in situ activation and coupling method described earlier [29].

### 2.2. Radiochemical synthesis

$^{64}\text{Cu}$  was obtained from Mallinckrodt Institute of Radiology, Washington University School of Medicine (St. Louis, MO, USA).  $^{64}\text{Cu}$  was produced in a CS-15 biomedical cyclotron using the  $^{64}\text{Ni(p,n)}^{64}\text{Cu}$  nuclear reaction, separated by the method of McCarthy et al. [31] and supplied in high specific activity as  $\text{CuCl}_2$  in 0.1 mol/L of HCl. The DOTA-[Lys<sup>3</sup>]BBN and the DOTA-Aca-BBN(7–4) conjugates were labeled with  $^{64}\text{Cu}$  using a modified protocol previously described. Approximately 7.5  $\mu\text{g}$  of the conjugate per mCi of  $^{64}\text{Cu}$  in 0.1N NaOAc (pH 6.0) buffer was used. The labeled compound was purified using a Dionex 680 chromatography system with Vydac protein and peptide columns and a UVD 170U absorbance detector and model 105S single-channel radiation detector (Carroll & Ramsey Associates, Berkeley, CA, USA). The gradient used is composed of solvent starting from 95% A (0.1% trifluoroacetic acid in

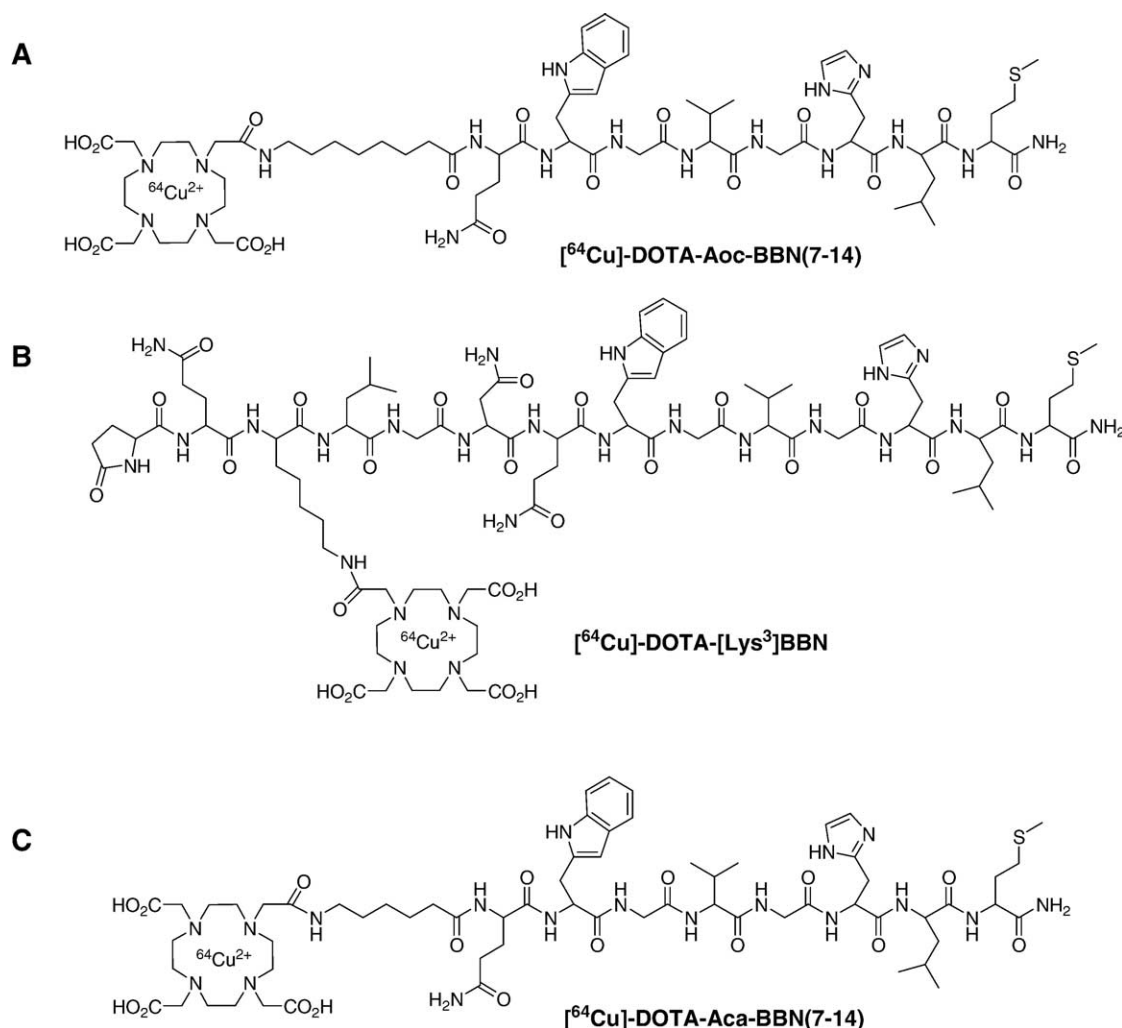


Fig. 1. Schematic structures of (A) [<sup>64</sup>Cu]-DOTA-Aoc-BBN(7-14) [30], (B) [<sup>64</sup>Cu]-DOTA-[Lys<sup>3</sup>]BBN and (C) [<sup>64</sup>Cu]-DOTA-Aca-BBN(7-14).

water) and 5% B [0.1% TFA in acetonitrile (CH<sub>3</sub>CN)] at 0–5 min to 35% A and 65% B at 35 min.

### 2.3. Cell culture

PC-3 and 22Rv1 human prostate adenocarcinoma cell lines obtained from the American Type Culture Collection (ATCC, Manassas, VA, USA) were cultured in monolayers in Ham's F-12K and RPMI 1640 media (Invitrogen, Grand Island, NY, USA), respectively, supplemented with 10% fetal bovine serum in a humidified atmosphere of 5% CO<sub>2</sub>/95% air at 37°C. After harvested by centrifuging, cells were resuspended either in pH 7.4 phosphate-buffered saline (PBS) containing 0.1% bovine serum albumin (BSA) for in vitro receptor binding assay or in fresh media for tumor inoculation on animals.

### 2.4. In vitro receptor binding assay

In vitro binding affinity and specificity of GRPR of BBN analogues and their DOTA conjugates were investigated using competitive receptor binding assay. [<sup>125</sup>I]-[Tyr<sup>4</sup>]BBN (Perkin-Elmer Life Science Products, Boston, MA, USA)

was used as the GRPR-specific radioligand. Experiments were performed on PC-3 and 22Rv1 human prostate cell lines using modified methods previously described [29]. PBS was used as binding buffer; and 0.1% BSA was added to minimize nonspecific binding. Serial dilution of BBN analogs and their DOTA conjugates ranging from 0 to 2000 nmol/L, 0.015 μCi (0.55Bq) of [<sup>125</sup>I]-[Tyr<sup>4</sup>]BBN in 50 μL binding buffer and 10<sup>5</sup> PC-3 cells or 2.5 × 10<sup>5</sup> 22Rv1 cells were used. The 50% inhibitory concentration (IC<sub>50</sub>) value for the displacement binding of [<sup>125</sup>I]-[Tyr<sup>4</sup>]BBN by those ligands was calculated by nonlinear regression analysis. Binding affinity assay of GRPR of [Tyr<sup>4</sup>]BBN on both PC-3 and 22Rv1 cell lines were also performed against [<sup>125</sup>I]-[Tyr<sup>4</sup>]BBN to estimate the K<sub>d</sub> (dissociation constant) and B<sub>max</sub> (GRPR receptor density on cell surface) value. A saturation binding curve and Scatchard transformation were obtained by nonlinear regression analysis, and the K<sub>d</sub> and B<sub>max</sub> values for both cells lines were extracted. GraphPad Prism 4.0 computer-fitting program (Graph-Pad Software, San Diego, CA, USA) was used. All the experiments were repeated twice with triplicate samples.

### 2.5. Internalization and efflux studies

Internalization and efflux of  $^{64}\text{Cu}$ -DOTA-[Lys<sup>3</sup>]BBN and  $^{64}\text{Cu}$ -DOTA-Aca-BBN(7-14) on PC-3 cells were investigated using a protocol modified from a previously described method [29]. Studies were conducted in well plates, and  $2 \times 10^5$  PC-3 cells and approximately  $5 \times 10^5$  cpm/0.1 ml  $^{64}\text{Cu}$ -labeled tracer were used. The activity from each well was measured using  $\gamma$ -counter (Packard, Meriden, CT, USA). The data were normalized as a percentage of the total amount of radioactivity added per cell.

### 2.6. Tumor implantation and animal care

Approval for the animal protocol used in this study was obtained from the Stanford University Institutional Animal Care and Use Committee. Athymic *nu/nu* male mice were used. At the age of 5–6 weeks with an average body weight of about 20–25 g, each animal was inoculated intradermally with  $10^7$  PC-3 cells on the right front flank and  $10^7$  22Rv1 cells on the left front flank. Animals were given autoclaved rodent diet and water ad libitum before and during the time of tumor growth. Tumor growth was monitored at least twice a week. Animal experiments were conducted when the tumors reached a diameter of approximately 4–6 mm at approximately 3–4 weeks after tumor implantation. The animals were sacrificed with excess  $\text{CO}_2$  gas once the tumor began to affect the mobility of the animals.

### 2.7. Metabolic stability

The metabolic stability of [ $^{64}\text{Cu}$ ]-DOTA-[Lys<sup>3</sup>]BBN and [ $^{64}\text{Cu}$ ]-DOTA-Aca-BBN(7-14) was evaluated using 3 animals for each tracer. Each animal was injected intravenously with approximately 300  $\mu\text{Ci}$  (11.1 MBq) of the radiotracer. The animals were euthanized and dissected at 0.5, 1 and 2 h post injection (p.i.) to collect blood, urine, tumor, liver and kidney samples. Blood and urine samples were immediately centrifuged at 12,000  $g$  for 5 min. Tumor, liver and kidney samples were homogenized, suspended in adequate amount of PBS and centrifuged at 16,000  $g$  for 5 min. For each sample, the supernatant was removed, and the pellet was washed with 500  $\mu\text{L}$  PBS. The activity of the pellet and the combined two supernatant solutions were measured using  $\gamma$ -counter. Extraction efficiency was determined by calculating the ratio of  $\text{cpm}_{\text{supernatant}}/(\text{cpm}_{\text{supernatant}} + \text{cpm}_{\text{pellet}})$ . The combined supernatant was passed through a Sep-Pak C<sub>18</sub> cartridge (Waters Corp., Milford, MA, USA). The cartridge was washed with 2 ml of water and eluted with 2 ml of  $\text{CH}_3\text{CN}/0.1\%$  TFA. The activity of the passing-through, water eluent and  $\text{CH}_3\text{CN}$  eluent was measured using  $\gamma$ -counter. The eluent efficiency was determined by calculating the ratio of  $(\text{cpm}_{\text{water}} + \text{cpm}_{\text{CH}_3\text{CN}})/(\text{cpm}_{\text{water}} + \text{cpm}_{\text{CH}_3\text{CN}} + \text{cpm}_{\text{passing-through}})$ . The water and  $\text{CH}_3\text{CN}$  eluents were dried with an  $\text{N}_2$  gas blowing and oil bath at  $40^\circ\text{C}$ . The residue was dissolved in 500  $\mu\text{L}$  PBS and injected onto radio-high-performance liquid chromatography (HPLC) equipped

with a Vydac protein and peptide column (218TP54; 5  $\mu\text{m}$ ,  $250 \times 4.6$  mm). The flow was 1 ml/min with a gradient of solvent described in the Radiochemical Synthesis section. The eluent was fraction-collected every 30 s, and the activity of each fraction was measured in a  $\gamma$ -counter. The data were plotted to reconstruct the HPLC spectrum.

### 2.8. MicroPET imaging

PET imaging was performed on a microPET R4 rodent model scanner (CTI Concorde Microsystems), and the imaging data were analyzed using ASIPro VM 5.2.4.0 (Acquisition Sinogram Image PROcessing using IDL's Virtual Machine). The scanner has a linear resolution of about 2.5 mm in all three dimensions to make an overall volumetric resolution of  $15.6 \text{ mm}^3$ . The raw list mode is reconstructed into images using a two-dimensional ordered subsets expectation maximum algorithm (OSEM). No correction is needed for attenuation or scatter. At each microPET scan, region of interests were drawn over each tumor, normal tissue and major organs on decay-corrected, whole-body coronal images and converted to an imaging ROI-derived percentage administered activity per gram of tissue (%ID/g) using a conversion factor of approximately 2000  $\mu\text{Ci}/\text{ml}$ . For each animal to be scanned, approximately 300  $\mu\text{Ci}$  (11.1 MBq) of activity was administered through tail-vein injection prior to anesthesia. Animals were anesthetized with 2% isoflurane at 0.2 L/min flow of oxygen and were then immediately placed onto the bed of the scanner, and the bed was positioned so that the center of field of view was at the spine adjacent to the tumor on the shoulder. The animal was close to the center of the field of view to obtain the highest resolution and sensitivity. Dynamic imaging was performed for 60 min with one frame of image collected for duration of 1 min, two frames for 2 min, 4 frames for 5 min, and five frames for 7 min (total of 12 frames). After data acquisition, animals were moved back to their housing cage for recovery. Additional static images were acquired at later time points. For these static data acquisition, animals were anesthetized with 2% isoflurane in oxygen, moved to the scanning bed immediately afterwards, and moved back to their housing cage after the scan until the next static image acquisition. Static images were collected for 10 min at 2 h and 4 h p.i. and for 30 min at 12 h and 18 h p.i.

### 2.9. Statistical analysis

The data were expressed as means  $\pm$  S.D. One-way analysis of variance was used for statistical evaluation. Means were compared using Student's *t* test.  $P < .05$  was considered significant.

## 3. Results

### 3.1. Chemical and radiochemical synthesis

With the excess amount of DOTA-SNHS, The DOTA-[Lys<sup>3</sup>]BBN conjugate was produced in  $>95\%$  yield. The



Table 1

Summary of (A) the IC<sub>50</sub> values for different ligands against PC-3 and 22Rv1 cell lines obtained from competitive binding assay using [<sup>125</sup>I]-[Tyr<sup>4</sup>]BBN; and (B) K<sub>d</sub> and B<sub>Max</sub> for PC-3 and 22Rv1 cell lines measured using [Tyr<sup>4</sup>]BBN obtained from the saturation binding curve using Scatchard transformation of the competitive binding curve

	PC-3	22Rv1
(A) IC <sub>50</sub> (nmol/L)		
[Lys <sup>3</sup> ]-BBN	3.3±0.4	NS <sup>a</sup>
DOTA-[Lys <sup>3</sup> ]-BBN	2.2±0.5	NS <sup>a</sup>
Aca-BBN(7-14)	20.8±0.3	NS <sup>a</sup>
DOTA-Aca-BBN(7-14)	18.4±0.2	NS <sup>a</sup>
(B)		
K <sub>d</sub> (nM)	14.8±0.4	NS <sup>a</sup>
B <sub>Max</sub> (receptors/cell)	2.70±0.1×10 <sup>6</sup>	NS <sup>a</sup>

<sup>a</sup> NS: readings from gamma-counter are not significant enough to extract a binding curve and associated parameters.

retention time of this compound on HPLC was 19.8 min using the solvent gradient, as described previously in the Materials and Methods section. An *m/z* of 1979 for [M+H]<sup>+</sup> was obtained using Matrix-assisted laser desorption ionization time-of-flight mass spectrometer. DOTA-Aca-BBN(7-14) conjugate was synthesized and characterized using the same method. The yield was >95%, the retention time on HPLC was 19.5 min and *m/z*=1439 for [M+H]<sup>+</sup>. Both DOTA-[Lys<sup>3</sup>]BBN and DOTA-Aca-BBN(7-14) (Fig. 1B and 1C) were labeled with <sup>64</sup>Cu in >90% radiochemical yield and >98% radiochemical purity with a retention time on HPLC of about 18.5 and 18.0 min, respectively. The compounds were used immediately for in vitro and in vivo assays and microPET imaging studies.

### 3.2. In vitro receptor binding assay

The binding affinity of [Lys<sup>3</sup>]BBN, Aca-BBN(7-14) and DOTA-Aca-BBN(7-14) for GRPR was evaluated for PC-3 and 22Rv1 human prostate adenocarcinoma cell lines. A typical sigmoid curve for the displacement of [<sup>125</sup>I]-[Tyr<sup>4</sup>]BBN from PC-3 cells as a function of increasing concentration of DOTA-Aca-BBN(7-14) was obtained. The IC<sub>50</sub> values (concentration required to have 50% inhibitory effect) were determined for all three different ligands on both PC-3 and 22Rv1 cells and are summarized in Table 1. The result for DOTA-[Lys<sup>3</sup>]BBN on PC-3 cells has been reported earlier [29] and was included for comparison. The IC<sub>50</sub> value was determined to be 3.3±0.4 nM for [Lys<sup>3</sup>]BBN and 20.8±0.3 nM for Aca-BBN(7-14) on 10<sup>5</sup> PC-3 cells. Conjugation with DOTA did not significantly alter the binding affinity for both compounds. The results showed the IC<sub>50</sub> values to be 2.2±0.5 and 18.4±0.2 nM for DOTA-[Lys<sup>3</sup>]BBN and DOTA-Aca-BBN(7-14), respectively. For 22Rv1, no significant binding characteristics could be obtained for any of the four compounds with the use of up to 2.5×10<sup>5</sup> cells. The binding affinity of [Tyr<sup>4</sup>]BBN for GRPR was also evaluated for PC-3 and 22Rv1 cell lines against [<sup>125</sup>I]-[Tyr<sup>4</sup>]BBN to estimate the receptor density on the cells. A sigmoid curve from PC-3 cells as a function of

increasing concentration of [Tyr<sup>4</sup>]BBN was obtained. The linear portion of the data was used to generate the Scatchard transformation. K<sub>d</sub> (the mean dissociation constant between the radioligand and the GRPR on the cell surface) of [<sup>125</sup>I]-[Tyr<sup>4</sup>]BBN against PC-3 cells was calculated to be 14.8±0.4 nM and B<sub>max</sub>, the density of GRPR on cell surface to be 2.7±0.1×10<sup>6</sup> receptors/cell. For 22Rv1, no significant binding affinity could be obtained.

### 3.3. Internalization and efflux studies

Results for the internalization of both tracers, [<sup>64</sup>Cu]-DOTA-[Lys<sup>3</sup>]BBN and [<sup>64</sup>Cu]-DOTA-Aca-BBN(7-14), are shown in Fig. 2A. For both tracers, internalization occurred immediately after the preincubation step (at 0 min of incubation): 55% for [<sup>64</sup>Cu]-DOTA-[Lys<sup>3</sup>]BBN and 60% for [<sup>64</sup>Cu]-DOTA-Aca-BBN(7-14). At approximately 20 min of incubation, internalization for both tracers reached a maximum [~84% for [<sup>64</sup>Cu]-DOTA-[Lys<sup>3</sup>]BBN and >75% for [<sup>64</sup>Cu]-DOTA-Aca-BBN(7-14)] and stayed saturated until 120 min of incubation.

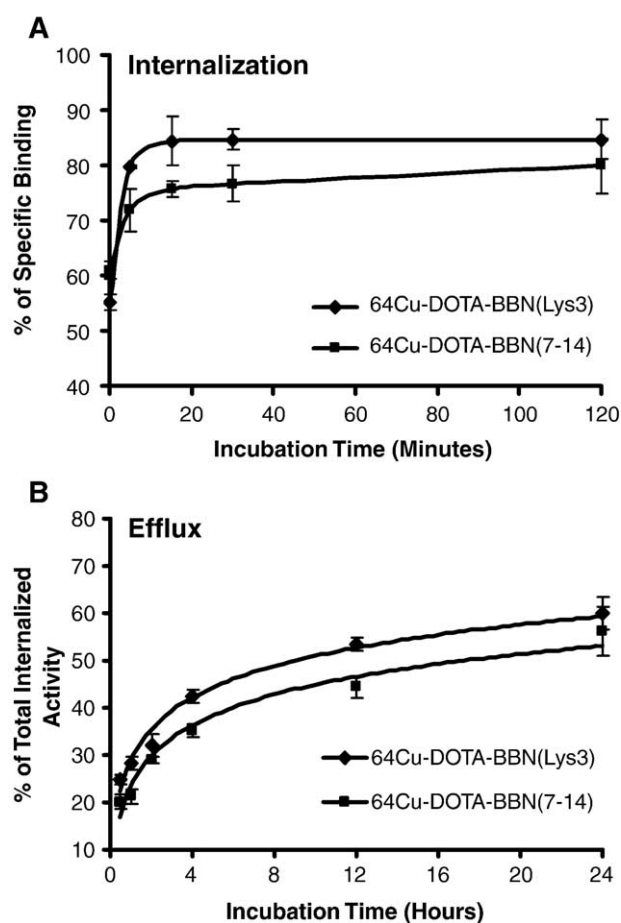


Fig. 2. (A) Time-dependent internalization and (B) time-dependent efflux of [<sup>64</sup>Cu]-DOTA-[Lys<sup>3</sup>]BBN (◆) and [<sup>64</sup>Cu]-DOTA-Aca-BBN(7-14) (■) by PC-3 cells. Data are percentage of acid-resistant (internalized) radioactivity in cells for internalization, and percentage of radioactivity remained in the culture media for efflux.

Table 2  
Summary of the extraction and elution efficiency from blood, urine, liver, kidney and PC-3 tumor collected at 30 and 60 minutes post intravenous injection of (A) [<sup>64</sup>Cu]-DOTA-[Lys<sup>3</sup>]-BBN and (B) [<sup>64</sup>Cu]-DOTA-Aca-BBN(7-14)

	Extraction efficiency (%)					Elution efficiency (%)				
	Blood	Urine	Liver	Kidney	Tumor	Blood	Urine	Liver	Kidney	Tumor
(A) [ <sup>64</sup> Cu]-DOTA-[Lys <sup>3</sup> ]-BBN										
30 min p.i.	92.7	N/A	78.3	70.7	76.9	94.4	96.0	84.6	88.6	88.0
60 min p.i.	87.6	N/A	71.5	60.8	85.3	95.9	97.0	90.3	88.9	95.9
(B) [ <sup>64</sup> Cu]-DOTA-Aca-BBN(7-14)										
30 min p.i.	97.8	N/A	93.9	89.6	81.6	93.6	90.7	88.7	84.5	75.0
60 min p.i.	96.1	N/A	90.5	89.6	85.8	96.1	92.8	84.6	83.8	80.3

Efflux studies were also carried out up to 24 h of incubation to further characterize both tracers (Fig. 2B). Both [<sup>64</sup>Cu]-DOTA-[Lys<sup>3</sup>]BBN and [<sup>64</sup>Cu]-DOTA-Aca-BBN(7-14) tracers showed a similar efflux curve: with 30 min of incubation, both tracers had approximately 20–25% efflux out of the PC-3 cells, followed by a ~15% increase up till 4 h of incubation. The efflux rate was decreased afterwards. Till the end of experiments with a 24 h incubation time, approximately 40% of the radiotracers remained in the cells.

3.4. Metabolism stability

The metabolic stability of [<sup>64</sup>Cu]-DOTA-[Lys<sup>3</sup>]BBN was determined in mouse blood, urine, tumor, liver and kidney

samples 30, 60 and 120 min p.i. (data not shown). Efficiency of extraction by homogenizing the organs and efficiency of elution are summarized in Table 2A, and Table 3A summarizes the relative integrated area of each individual peaks in percentage for [<sup>64</sup>Cu]-DOTA-[Lys<sup>3</sup>]BBN. HPLC of the radio-labeled tracer performed immediately prior to the injection showed a single peak (100% area) with a retention time of 18.5 min. This spectrum was used as the 0-min time point for blood, urine and all the organ samples. At 30 min p.i., approximately 78% of the intact tracer was retained in the blood and a new peak at about 5 min showed up with 22% area. Approximately 65% of the intact tracer was detected in tumor along with the second metabolite at 6 min. Liver had about 65% of

Table 3  
Summary of data from the HPLC profiles from the soluble fraction of blood and urine samples and organ homogenates 0 (immediately prior to injection), 30 and 60 minutes post intravenous injection of (A) [<sup>64</sup>Cu]-DOTA-[Lys<sup>3</sup>]-BBN and (B) [<sup>64</sup>Cu]-DOTA-Aca-BBN(7-14)

Time p.i. (min)	Blood		Urine		Tumor		Liver		Kidney	
	Elution time (min)	Area (%)	Elution time (min)	Area (%)	Elution time (min)	Area (%)	Elution time (min)	Area (%)	Elution time (min)	Area (%)
(A)										
0	18.5	100	18.5	100	18.5	100	18.5	100	18.5	100
30	18.5	78.0			18.5	64.6	18.5	65.4	18.5	25.9
	5.0	22.0	5.0	100	6.0	35.4	14.0 4.0	23.4 11.2	4.0	72.1
60	18.5	58.4			18.5	23.1	18.5	39.9	18.5	17.4
							14.0	43.4		
	3.0	42.6	3.0 4.0	65.2 34.8	6.0	76.9	4.0	16.7	4.0	82.6
(B)										
0	18.0	100	18.0	100	18.0	100	18.0	100	18.0	100
30	19.0	68.1					19.0	20.1	19.5	45.2
			14.5	39.4	14.5	65.3	15.0	45.3		
	5.5	21.4	5.0	60.6	4.0	34.7	4.0	33.5	4.0	51.9
60	4.0	10.5								
	18.5	14.2								
					14.5	56.9	13.5	45.1		
	6.0	41.4	4.0	100	4.0	43.1	5.0	52.9	4.0	100
	3.5	44.8								

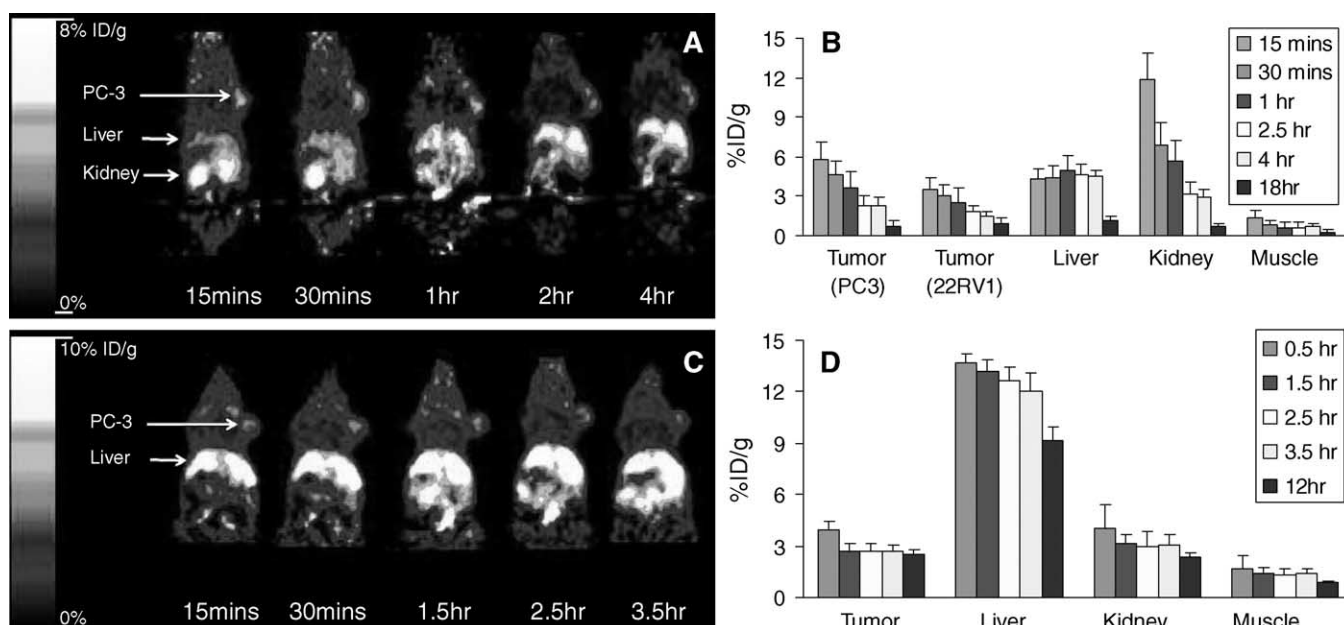


Fig. 3. MicroPET images of athymic nude mice with PC-3 tumor on the right shoulder. Coronal images (decayed corrected to time of injection) were collected at multiple time points post radiotracer  $[^{64}\text{Cu}]\text{-DOTA-}[\text{Lys}^3]\text{BBN}$  (300  $\mu\text{Ci}$ , 11.1 MBq) (A) or  $[^{64}\text{Cu}]\text{-DOTA-Aca-BBN(7-14)}$  (C) injection. Major organ and tumor distribution data derived from quantitative microPET imaging studies for  $[^{64}\text{Cu}]\text{-DOTA-}[\text{Lys}^3]\text{BBN}$  (B) and  $[^{64}\text{Cu}]\text{-DOTA-Aca-BBN(7-14)}$  (D) were also shown ( $n=3$ ). Time indicated in all panels refers to the time point of scan initiation.

the intact tracer, and in addition to the metabolite eluted at early time (4.0 min, 12%), a third peak was observable at 14 min with an area of about 23%. For kidneys, there was less than 30% of the intact tracer found. The major peak (72%) was observed at 4 min. A complete metabolism was observed in urine (100% area at 5.0 min).

HPLC at 60 min p.i. showed an increasing area for the early time eluent(s), indicating that the tracer had been further metabolized. For blood, the intact tracer decreased to <60%, and it further dropped to 23%, 40% and 17% in tumor, liver and kidneys, respectively. The second metabolite eluted at about 14 min for liver remained observable with an increasing area (from 23% to 43%). In urine, two peaks were observed at 3 and 4 min, likely to be new metabolites derived from the one eluted at 5 min at 30 min p.i. HPLC for samples collected at 120 min p.i. showed further decomposition of the radio-labeled tracer (data not shown).

The metabolic stability of  $[^{64}\text{Cu}]\text{-DOTA-Aca-BBN(7-14)}$  was also determined in mouse blood, urine, tumor, liver and kidney samples 30 and 60 min p.i. using the same protocol. Efficiency of extraction by homogenizing the organs was 97.8% to 81.6%, and efficiency of elution was between 96.1% and 75.0%, as shown in Table 2B. Table 3B summarizes the relative integrated area for each individual peaks in percentage for  $[^{64}\text{Cu}]\text{-DOTA-Aca-BBN(7-14)}$ . HPLC of the radio-labeled tracer was performed immediately before the tracer injection as the 0-min data point for all five extractants. It showed that the intact tracer had an elution time of approximately 18 min. HPLC of those samples were performed, eluents were collected every 30 s

for gamma counting and the HPLC spectra were reconstructed using the counting results for 30 and 60 min.

At 30 min p.i., the peak for intact tracer was not observable in any of the five samples. Blood sample showed two broad bands at 19.5 (68%) and at 4–5 min (total 32%). Urine and PC-3 tumor samples showed one peak at 14.5 min and another weak peak at 4–5 min with higher intensity. Liver and kidney samples showed a group of broad bands with identifiable peaks at about 19, 15 (major peak for liver, 45% area) and 4 min (major peak for kidney, 52% area). At 60 min and 120 min (data not shown) p.i., HPLC spectra showed a further metabolism for the injected radio-tracer with no sign of the intact tracer at 18.0 min retention time. Peaks at areas of low retention time showed increased percent area. For blood and liver, broader band consisted of multiple peaks was also observed.

Together, these results for both  $[^{64}\text{Cu}]\text{-DOTA-}[\text{Lys}^3]\text{BBN}$  and  $[^{64}\text{Cu}]\text{-DOTA-Aca-BBN(7-14)}$  showed that  $[^{64}\text{Cu}]\text{-DOTA-Aca-BBN(7-14)}$  has extremely low metabolic stability as the tracer decomposed sooner than 30 min after being injected. Alternatively,  $[^{64}\text{Cu}]\text{-DOTA-}[\text{Lys}^3]\text{BBN}$  showed a moderate metabolic stability. At 60 min p.i., approximately 23% of the tracer remained in the tumor. Further work has yet to be accomplished to identify the metabolites observed in these experiments.

### 3.5. MicroPET imaging

Fig. 3A showed a series of microPET images of a nude mouse bearing PC-3 tumor on the right shoulder and 22Rv1 tumor on the left shoulder (not seen from the coronal images shown) after injecting approximately 300  $\mu\text{Ci}$  (11.1 MBq)

of [ $^{64}\text{Cu}$ ]-DOTA-[Lys<sup>3</sup>]BBN. The data were collected using a dynamic sequence from 0 to 60 min, and a static sequence at 2, 4, 12 and 18 h p.i (data acquisition protocol was described in the Materials and Methods section). Quantification of tracer uptake in %ID/g was calculated and shown in Fig. 3B. It has been shown that tracer uptake calculated from noninvasive microPET imaging is comparable to that obtained from direct tissue sampling [29]. Uptake of [ $^{64}\text{Cu}$ ]-DOTA-[Lys<sup>3</sup>]BBN occurred immediately after injection for both tumors and all the organs. Maximum uptake was observed at 15 min for both tumors, kidneys and muscle. Uptake in the liver reached its maximum level at about 1 h p.i. Uptake in PC-3 tumor is higher than that in 22Rv1 tumor (%ID/g=5.8 for PC-3 and 3.49,  $P<.01$ ), demonstrating that this tracer was able to target the GRPR whose expression level is high in PC-3 but low in 22Rv1 tumor. It also should be noted that kidney uptake was the highest among all the ROIs studied here, suggesting that excretion through the kidney/urine is likely to be the pathway for this tracer to be metabolized.

Significant difference in uptake behavior was observed for [ $^{64}\text{Cu}$ ]-DOTA-Aca-BBN(7-14) compared to that for [ $^{64}\text{Cu}$ ]-DOTA-[Lys<sup>3</sup>]BBN (Fig. 3C and D). Uptake on PC-3 tumor reached maximum (4.63%) at around 5 min post injection and remained to be below 3% after 30 min post injection. Liver uptake was significantly higher than that for other organs and remained as high as 9%ID/g at 12 h p.i. Renal uptake was significantly lower than that for the previous tracer [ $^{64}\text{Cu}$ ]-DOTA-[Lys<sup>3</sup>]BBN. When [ $^{64}\text{Cu}$ ]-DOTA-Aca-BBN(7-14) was coinjected with blocking dose of [Tyr<sup>4</sup>]BBN (10 mg/kg), the activity accumulations in the PC-3 tumor and pancreas were partially inhibited, reflecting the low receptor affinity of the truncated peptide tracer (data not shown).

#### 4. Discussion

Imaging evaluation of prostate cancer continues to be challenging. Current imaging tests, including ultrasound, computed tomography, magnetic resonance imaging and  $^{111}\text{In}$ -capromab pendetide (ProstaScint) are not sufficient for exact estimation of the initial tumor stage, detection of local recurrence or metastatic disease. Due to the low proliferation rate of prostate cancer,  $^{18}\text{F}$ -FDG accumulation in the primary prostate cancer is generally low, although it might be useful in the evaluation of advanced AI disease and in patients with high Gleason scores and serum PSA level, in the detection of active osseous and soft tissue metastases and in the assessment of response after androgen ablation and chemotherapies [34,35].  $^{11}\text{C}$ -acetate and  $^{18}\text{F}$ - or  $^{11}\text{C}$ -labeled choline appear to be more or less equally useful in imaging prostate cancer and more advantageous than fluorodeoxyglucose in some clinical circumstances [36–38]. Overexpression of cell surface GRPR protein in a large variety of human tumors, including AI prostate cancers, provides the basis for suitably radiolabeled BBN

analogues for measurement of GRP receptor occurrence and may be helpful in choosing the method of diagnosis and treatment, as well as in better understanding the pathophysiology of prostate cancer.

For those BBN analogues that have been studied, they can be categorized to two different types based on their structures. Type A includes analogues that have been truncated and only a portion [usually BBN(7-14)] of the peptide was retained. Type B includes analogues that have a full length, while one or more amino acid residues were selectively replaced. It is generally recognized that the C-terminus is involved in receptor binding and could be more stable than the full-length tetradecapeptide. We found that truncated peptide sequence had lower receptor affinity than [Lys<sup>3</sup>]BBN and that  $^{64}\text{Cu}$ -DOTA-Aca-BBN(7-14) is less metabolically stable than  $^{64}\text{Cu}$ -DOTA-[Lys<sup>3</sup>]BBN (Table 3). The half-life in blood as estimated from the extractable fragment was about 1.7 h for [Lys<sup>3</sup>]BBN and was less than 5 min for BBN(7-14). HPLC analysis of the metabolites along with coinjection of the predefined metabolites is needed to identify the degradation products. The knowledge of the cleavage sites and the characterization of the metabolites are of importance because this knowledge will allow us to define and synthesize peptides of enhanced metabolic stability. The excessive hepatobiliary excretion of the truncated peptide should also be given particular attention, given that several proposed GRPR-seeking radiotracers are based on the BBN(7-14) lipophilic motif and are reported to lead to excessive intestinal radioactivity. This effect, in combination with the poor metabolic stability of the truncated sequence, may hamper the detection of tumor deposits in the abdomen.

Internalization of  $^{64}\text{Cu}$ -DOTA-[Lys<sup>3</sup>]BBN into PC-3 cells suggest an agonistic nature of the peptide. The rapid and high internalization (–80% of total cell-associated activity) was endocytosed within 15 min, which is independent from the peptide-to-receptor ratio (data not shown). Efflux of  $^{64}\text{Cu}$  activity from PC-3 cells after internalization of labeled [Lys<sup>3</sup>]BBN showed half-lives of about 12 h, which is much longer than that of  $^{125}\text{I}$ -[Tyr<sup>4</sup>]BBN [19]. The prolonged intracellular retention of  $^{64}\text{Cu}$  in tumor cells is most likely due to the lack of cell permeability of the DOTA conjugate and is not related to the metabolized peptide fractions.

In addition to PC-3 tumor, pancreas and intestine have also been reported to be organs with high expression of GRPR. The high pancreatic and tumor uptakes were effectively reduced in the animals receiving coinjection of 2 mg/kg of [Lys<sup>3</sup>]BBN. Further increase of blocking dose of [Lys<sup>3</sup>]BBN had minimal effect on the biodistribution pattern. Different from previous report using [ $^{99\text{m}}\text{Tc}$ ]demobesin 1 [28], nonradiolabeled BBN failed to reduce the uptake of  $^{64}\text{Cu}$ -DOTA-[Lys<sup>3</sup>]BBN in the intestinal tract. The high receptor-mediated tracer uptake in the pancreas is a major concern for limiting dose calculations. Further reduction of the hepatobiliary clearance is also necessary to



lower the background radioactivity for better imaging of BBN-/GRPR-positive cancers and their metastases located in the abdominal area.

The predominant excretion pathway of  $^{64}\text{Cu}$ -DOTA-[Lys<sup>3</sup>]BBN is through the kidneys into the urine, wherein around 70–80 %ID was collected within the first 30 min. All radioactivity found in the urine is in the form of two major metabolites, with no traces of intact  $^{64}\text{Cu}$ -DOTA-[Lys<sup>3</sup>]BBN present.  $^{64}\text{Cu}$ -DOTA-[Lys<sup>3</sup>]BBN is not stable during incubation in murine plasma either (data not shown). Less than 40% of intact peptide tracer was detectable after 30 min and less than 2% left after 20-h incubation. The metabolites seem to form mainly in the kidneys as only 26% intact tracer at 30 min p.i. and 17% at 1 h p.i. The persistent renal activity accumulation may be explained by the fact that the radiolabeled peptide was filtered by the renal glomerulus and following interaction with anionic charges on cell membranes.

Recently, a cross-bridged ligand tetraazamacrocyclic 4,11-bis(carboxymethoxymethyl)-1,4,8,11-tetraazabicyclo (6.6.2)hexadecane (CB-TE2A) was developed and found to have improved kinetic stability both in vitro and in vivo compared with DOTA and TETA complexes [39–42]. In particular, direct comparison between  $^{64}\text{Cu}$ -CB-TE2A-Y3-TATE and  $^{64}\text{Cu}$ -TETA-Y3-TATE for microPET imaging of somatostatin receptor-positive tumors showed increased tumor detection sensitivity of the cross-bridge peptide complex. We suggest that  $^{64}\text{Cu}$ -CB-TE2A-[Lys<sup>3</sup>]BBN may be more kinetically inert and results in additional improvement in tumor targeting and in vivo kinetics, as compared to the title compound evaluated in this study.

Despite the success of  $^{64}\text{Cu}$ -DOTA-[Lys<sup>3</sup>]BBN to detect GRPR positive PC-3 tumor in a subcutaneous xenograft model, it is unknown whether the same tracer can be applied to visualize orthotopic prostate cancer model. The background signal in the intestinal tract and rapid clearance of metabolized radioligand into the urinary bladder may significantly interfere with the receptor-mediated activity accumulation in the prostate gland. It is also unknown whether the same tracer can be applied to delineate prostate cancer bone and lymph node metastases.

## 5. Conclusion

In conclusion, the data presented suggests that  $^{64}\text{Cu}$ -DOTA-[Lys<sup>3</sup>]BBN has high affinity for GRPR and moderate metabolic stability, results in specific tumor localization and exhibits good imaging characteristics with good tumor-to-background ratios.  $^{64}\text{Cu}$ -DOTA-[Lys<sup>3</sup>]BBN is also superior to  $^{64}\text{Cu}$ -DOTA-Aca-BBN(7-14) for GRPR-positive tumor targeting.  $^{64}\text{Cu}$ -DOTA-[Lys<sup>3</sup>]BBN has the potential to be translated into clinical settings in healthy volunteers for defining tracer biodistribution, stability, pharmacokinetics and radiation dosimetry and in cancer patients for lesion detection and quantification of GRPR level.

## Acknowledgments

Supported, in part, by DOD Prostate Cancer Research Program (PCRP) New Investigator Award (NIA) DAMD1717-03-1-0143, National Cancer Institute (NCI) Grant R21 CA102123, National Institute of Biomedical Imaging and Bioengineering (NIBIB) Grant R21 EB001785, Department of Defense (DOD) Breast Cancer Research Program (BCRP) Concept Award DAMD17-03-1-0752, DOD BCRP IDEA Award W81XWH-04-1-0697, American Lung Association California (ALAC), the Society of Nuclear Medicine Education and Research Foundation, National Cancer Institute (NCI) Small Animal Imaging Resource Program (SAIRP) R24 CA93862, NCI In Vivo Cellular Molecular Imaging Center (ICMIC) grant P50 CA114747, and NCI Centers of Cancer Nanotechnology Excellence (CCNE) U54 grant. The production of Cu-64 at Washington University School of Medicine is supported by the NCI grant R24 CA86307.

## References

- [1] Jemal A, Ward E, Thun MJ. Contemporary lung cancer trends among U.S. women. *Cancer Epidemiol Biomarkers Prev* 2005;14: 582–5.
- [2] Kessler B, Albertsen P. The natural history of prostate cancer. *Urol Clin North Am* 2003;30:219–26.
- [3] Jenster G. The role of the androgen receptor in the development and progression of prostate cancer. *Semin Oncol* 1999;26:407–21.
- [4] Sunday ME, Wolfe HJ, Roos BA, Chin WW, Spindel ER. Gastrin-releasing peptide gene expression in developing, hyperplastic, and neoplastic human thyroid C-cells. *Endocrinology* 1988;122: 1551–8.
- [5] Guo YS, Townsend Jr CM. Roles of gastrointestinal hormones in pancreatic cancer. *J Hepatobiliary Pancreat Surg* 2000;7:276–85.
- [6] Scott N, Millward E, Cartwright EJ, Preston SR, Coletta PL. Gastrin releasing peptide and gastrin releasing peptide receptor expression in gastrointestinal carcinoid tumours. *J Clin Pathol* 2004;57:189–92.
- [7] Glover SC, Tretiakova MS, Carroll RE, Benya RV. Increased frequency of gastrin-releasing peptide receptor gene mutations during colon-adenocarcinoma progression. *Mol Carcinog* 2003;37:5–15.
- [8] Scopinaro F, Varvarigou AD, Ussof W, De Vincentis G, Sourlingas TG, Evangelatos GP, et al. Technetium labeled bombesin-like peptide: preliminary report on breast cancer uptake in patients. *Cancer Biother Radiopharm* 2002;17:327–35.
- [9] Sun B, Halmos G, Schally AV, Wang X, Martinez M. Presence of receptors for bombesin/gastrin-releasing peptide and mRNA for three receptor subtypes in human prostate cancers. *Prostate* 2000;42: 295–303.
- [10] Williams BY, Schonbrunn A. Bombesin receptors in a human duodenal tumor cell line: binding properties and function. *Cancer Res* 1994;54:818–24.
- [11] Chung DH, Evers BM, Beauchamp RD, Upp Jr JR, Rajaraman S, Townsend Jr CM, et al. Bombesin stimulates growth of human gastrinoma. *Surgery* 1992;112:1059–65.
- [12] Bologna M, Festuccia C, Muzi P, Biordi L, Ciomei M. Bombesin stimulates growth of human prostatic cancer cells in vitro. *Cancer* 1989;63:1714–20.
- [13] Aprikian AG, Han K, Guy L, Landry F, Begin LR, Chevalier S. Neuroendocrine differentiation and the bombesin/gastrin-releasing peptide family of neuropeptides in the progression of human prostate cancer. *Prostate Suppl* 1998;8:52–61.

- [14] Jongsma J, Oomen MH, Noordzij MA, Romijn JC, van Der Kwast TH, Schroder FH, et al. Androgen-independent growth is induced by neuropeptides in human prostate cancer cell lines. *Prostate* 2000;42:34–44.
- [15] Koppan M, Halmos G, Arencibia JM, Lamharzi N, Schally AV. Bombesin/gastrin-releasing peptide antagonists RC-3095 and RC-3940-II inhibit tumor growth and decrease the levels and mRNA expression of epidermal growth factor receptors in H-69 small cell lung carcinoma. *Cancer* 1998;83:1335–43.
- [16] Szepeshazi K, Halmos G, Schally AV, Arencibia JM, Groot K, Vadillo-Buenfil M, et al. Growth inhibition of experimental pancreatic cancers and sustained reduction in epidermal growth factor receptors during therapy with hormonal peptide analogs. *J Cancer Res Clin Oncol* 1999;125:444–52.
- [17] Zhou J, Chen J, Mokotoff M, Ball ED. Targeting gastrin-releasing peptide receptors for cancer treatment. *Anticancer Drugs* 2004;15: 921–7.
- [18] Schally AV, Nagy A. Chemotherapy targeted to cancers through tumoral hormone receptors. *Trends Endocrinol Metab* 2004;15:300–10.
- [19] Smith CJ, Volkert WA, Hoffman TJ. Gastrin releasing peptide (GRP) receptor targeted radiopharmaceuticals: a concise update. *Nucl Med Biol* 2003;30:861–8.
- [20] Scheffel U, Pomper MG. PET imaging of GRP receptor expression in prostate cancer. *J Nucl Med* 2004;45:1277–8.
- [21] Varvarigou A, Bouziotis P, Zikos C, Scopinaro F, De Vincentis G. Gastrin-releasing peptide (GRP) analogues for cancer imaging. *Cancer Biother Radiopharm* 2004;19:219–29.
- [22] Van de Wiele C, Dumont F, van Belle S, Slegers G, Peers SH, Dierckx RA. Is there a role for agonist gastrin-releasing peptide receptor radioligands in tumour imaging? *Nucl Med Commun* 2001;22:5–15.
- [23] Krenning EP, Kwekkeboom DJ, Valkema R, Pauwels S, Kvoles LK, De Jong M, et al. Peptide receptor radionuclide therapy. *Ann N Y Acad Sci* 2004;1014:234–5.
- [24] Maecke HR, Hofmann M, Haberkorn U.  $^{68}\text{Ga}$ -labeled peptides in tumor imaging. *J Nucl Med* 2005;46(Suppl 1):172S–8S.
- [25] Van de Wiele C, Dumont F, Dierckx RA, Peers SH, Thornback JR, Slegers G, et al. Biodistribution and dosimetry of  $^{99\text{m}}\text{Tc}$ -RP527, a gastrin-releasing peptide (GRP) agonist for the visualization of GRP receptor-expressing malignancies. *J Nucl Med* 2001;42:1722–7.
- [26] Van de Wiele C, Dumont F, Vanden Broecke R, Oosterlinck W, Cocquyt V, Serreyn R, et al. Technetium-99m RP527, a GRP analogue for visualisation of GRP receptor-expressing malignancies: a feasibility study. *Eur J Nucl Med* 2000;27:1694–9.
- [27] Shao Y, Cherry SR, Farahani K, Meadors K, Siegel S, Silverman RW, et al. Simultaneous PET and MR imaging. *Phys Med Biol* 1997;42:1965–70.
- [28] Schuhmacher J, Zhang H, Doll J, Macke HR, Matys R, Hauser H, et al. GRP receptor-targeted PET of a rat pancreas carcinoma xenograft in nude mice with a  $^{68}\text{Ga}$ -labeled bombesin(6-14) analog. *J Nucl Med* 2005;46:691–9.
- [29] Chen X, Park R, Hou Y, Tohme M, Shahinian AH, Bading JR, et al. MicroPET and autoradiographic imaging of GRP receptor expression with  $^{64}\text{Cu}$ -DOTA-[Lys<sup>3</sup>]bombesin in human prostate adenocarcinoma xenografts. *J Nucl Med* 2004;45:1390–7.
- [30] Rogers BE, Bigott HM, McCarthy DW, Della Manna D, Kim J, Sharp TL, et al. MicroPET imaging of a gastrin-releasing peptide receptor-positive tumor in a mouse model of human prostate cancer using a  $^{64}\text{Cu}$ -labeled bombesin analogue. *Bioconjug Chem* 2003;14:756–63.
- [31] McCarthy DW, Shefer RE, Klinkowstein RE, Bass LA, Margeneau WH, Cutler CS, et al. Efficient production of high specific activity  $^{64}\text{Cu}$  using a biomedical cyclotron. *Nucl Med Biol* 1997;24:35–43.
- [32] Lewis JS, Lewis MR, Cutler PD, Srinivasan A, Schmidt MA, Schwarz SW, et al. Radiotherapy and dosimetry of  $^{64}\text{Cu}$ -TETA-Tyr<sup>3</sup>-octreotate in a somatostatin receptor-positive, tumor-bearing rat model. *Clin Cancer Res* 1999;5:3608–16.
- [33] Rogers BE, Manna DD, Safavy A, et al. In vitro and in vivo evaluation of a  $^{64}\text{Cu}$ -labeled polyethylene glycol-bombesin conjugate. *Cancer Biother Radiopharm* 2004;19:25–34.
- [34] Yaghoubi S, Barrio JR, Dahlbom M, Iyer M, Namavari M, Satyamurthy N, et al. Human pharmacokinetic and dosimetry studies of [ $^{18}\text{F}$ ]FHBG: a reporter probe for imaging herpes simplex virus type-1 thymidine kinase reporter gene expression. *J Nucl Med* 2001;42:1225–34.
- [35] Schoder H, Larson SM. Positron emission tomography for prostate, bladder, and renal cancer. *Semin Nucl Med* 2004;34:274–92.
- [36] Kwee SA, Coel MN, Lim J, Ko JP. Prostate cancer localization with  $^{18}\text{F}$  fluorine fluorocholine positron emission tomography. *J Urol* 2005;173:252–5.
- [37] Yamaguchi T, Lee J, Uemura H, Sasaki T, Takahashi N, Oka T, et al. Prostate cancer: a comparative study of  $^{11}\text{C}$ -choline PET and MR imaging combined with proton MR spectroscopy. *Eur J Nucl Med Mol Imaging* 2005;32:742–8.
- [38] Seltzer MA, Jahan SA, Sparks R, Stout DB, Satyamurthy N, Dahlbom M, et al. Radiation dose estimates in humans for  $^{11}\text{C}$ -acetate whole-body PET. *J Nucl Med* 2004;45:1233–6.
- [39] Boswell CA, Sun X, Niu W, Weisman GR, Wong EH, Rheingold AL, et al. Comparative in vivo stability of copper-64-labeled cross-bridged and conventional tetraazamacrocyclic complexes. *J Med Chem* 2004;47:1465–74.
- [40] Sprague JE, Peng Y, Sun X, Weisman GR, Wong EH, et al. Preparation and biological evaluation of copper-64-labeled tyr<sup>3</sup>-octreotate using a cross-bridged macrocyclic chelator. *Clin Cancer Res* 2004;10:8674–82.
- [41] Wong EH, Weisman GR, Hill DC, Reed DP, Rogers ME, Condon JS, et al. Synthesis and characterization of cross-bridged cyclams and pendant-armed derivatives and structural studies of their copper(II) complexes. *J Am Chem Soc* 2000;122:10561–72.
- [42] Sun X, Wuest M, Weisman GR, Wong EH, Reed DP, Boswell CA, et al. Radiolabeling and in vivo behavior of copper-64-labeled cross-bridged cyclam ligands. *J Med Chem* 2002;45:469–77.